A Reproduced Copy

OF

N66 – 23680

JET PROPULSION LABORATORY
CALIFORNIA INSTITUTE OF TECHNOLOGY
PASADENA, CALIFORNIA

RE-ORDER NO. 66-102

Quarterly Progress Report - 13 November 1965
to 13 February 1966

HIGH-PERFORMANCE THERMIONIC CONVERTER

Prepared for
Jet Propulsion Laboratory
California Institute of Technology
4800 Oak Grove Drive
Pasadena, California
Attention: Mr. Jack L. Flatley, Contract Negotiator

Contract 951225

EOS Report 6952-Q-3

15 February 1966

Prepared by
A. E. Campbell
D. H. Pollock
R. W. Hamerdinger
D. G. Worden

Approved by

A. O. Jensen, Manager
ELECTRO-OPTICAL TECHNOLOGY LABORATORY

Approved by

George R. White

George R. White, Manager
OPTICAL-ELECTRONICS GROUP

ELECTRO-OPTICAL SYSTEMS, INC. — PASADENA, CALIFORNIA
A Subsidiary of Xerox Corporation

This work was performed for the Jet Propulsion Laboratory, California Institute of Technology, sponsored by the National Aeronautics and Space Administration under Contract NAS7-100.

CONTENTS

CONTENTS (contd)

ILLUSTRATIONS

ILLUSTRATIONS (contd)

1. INTRODUCTION

This is the third quarterly report of progress on JPL Contract 951225, a program to (1) investigate basic materials, processes, and operating parameters affecting the stability and optimization of cesium-vapor thermionic converters, and (2) apply the results of these investigations to the fabrication of practical, high-performance, high-efficiency, long-life cesium-vapor thermionic converters.

1.1 Program Goals

The program goals are: (1) to generate fundamental data on the various converter operational parameters such as interelectrode spacing, Langmuir-Taylor type cesiated electron emission and work function of various electrode materials, and to establish optimum electrode materials processing, all to be applicable to practical cesium-vapor thermionic converters; (2) to conduct auxiliary experiments pertinent to the engineering design and converter fabrication in a manner such that the results are applicable to practical, high-efficiency, long-life cesium-vapor thermionic converters, and (3) to design, fabricate, and test a maximum of six cesium-vapor thermionic converters utilizing the results of the auxiliary experiments, leading to a performance of 20 watts/cm^2 at 0.8 volt output and an efficiency exceeding 14 percent for an emitter temperature of 1735^{o}C.

Adequate attention will be accorded the collector and radiator heat-transfer problems so that a converter with a 2-cm^2 emitter having an output of 40 watts at 0.8 volt can be fabricated with a minimum radiator weight. The weight of the converters must be consistent with the achievement of a four-converter generator weighing less than 4 pounds. The radiator area of the converters must be such that no additional cooling (such as excessive thermal conduction down the collector lead straps) is necessary for operation of the converter at its design conditions.

1.2 Summary of Work Performed During Reporting Period

During this past reporting period, precision data obtained from the variable parameter vehicle have substantiated and extended the measurements of the optimum pressure-distance (pd) relationships for a cesium vapor thermionic converter reported previously for lower temperature converters. These data have confirmed the predictions that an interelectrode spacing of approximately four mils (0.004 inch) is required for optimum converter operation at 0.8V dc utilizing polycrystalline rhenium electrodes. The operation of a converter in the close spaced region (less than 0.0005 inch interelectrode spacing) was examined in greater detail than previously reported and the expectation of high dc performance in this region was verified.

Extensive dc converter optimization data was obtained as a function of interelectrode spacing, collector root and cesium reservoir temperature for a constant emitter temperature of 1735°C. Sufficient dc data points were taken to precisely identify the optimum inter-relationships of these variables for optimum Re-Re converter operation.

The saturated electron emission was measured from cesiated polycrystalline rhenium emitters and collectors. Three separate cesium reservoir temperatures were examined for emitter temperatures covering the range from 2100°K to 1000°K. Bare work function measurements of the emitter were obtained in the high temperature range.

Heat transfer measurements were obtained which pertain to thermal conduction in cesium vapor. Two cesium pressure regions of interest were examined: first, the pressure region where the cesium atom-atom mean free path is greater than the interelectrode spacing (for vapor pressures of interest to converters this requires spacings of approximately 0.0002 inch); second, the pressure region where the cesium atom-atom mean free path is less than the interelectrode spacing.

During this report period, two secondary converter experiments were concluded. The first experiment involved the direct

optical measurement of the interelectrode spacing as a function of element temperature for a converter mockup. The spacing data obtained from the mockup compared favorably with values of the spacing calculated from the thermal expansion of the converter members. The second experiment established the feasibility of electron-beam welding prefabricated ceramic-metal seals directly to thermionic converter subassemblies.

1.3 Summary of Significant Results and Conclusions

The following significant results were achieved during this past quarterly report period:

1. Cesium-vapor converter output as a function of interelectrode spacing was accurately characterized over a spacing range encompassing the four different regions of converter operation: space-charge limited region, the onset or incipient breakdown region, the optimum pd region, and the fully developed positive column region. The measurements were made under dc steady-state conditions utilizing 0.1 percent accurate meters. The spacing measurements were made with $\pm$ 0.0001 inch accuracy.
2. The optimum cesium pressure-interelectrode distance product, pd, was precisely measured for two different cesium pressures. An optimum p x d value of 16 mil-Torr. was obtained for a polycrystalline rhenium electrode converter operating at a true emitter temperature of 1735^{o}C.
3. Langmuir-Taylor S type curves were obtained for cesiated polycrystalline rhenium. Measured saturated emission densities as high as 180 amps/cm^2 were obtained. Minimum cesiated rhenium work functions of 1.45 - 1.47 ev were obtained. The bare work function of the rhenium emitter used in the measurements was approximately 4.75 ev.

4. Precision cesium conduction heat transfer data was obtained. The results agree with classical heat transfer theory and with the semi-empirical analyses of vapor transport.
5. The variable parameter vehicle has undergone 700 hours of continuous operation without variation in measured quantities. Converter optimization data has been reproducible to within milliwatts of power output over this test time. At 0.8V dc, the maximum power output at an emitter temperature of 1735°C true, is 15.6 watts/cm^2.
6. A thermal mockup of a thermionic converter was operated in a manner to provide a direct, optical measurement of the interelectrode spacing. These spacing measurements agree to within 8 percent with values of spacing calculated from thermal expansion considerations.

2. VARIABLE PARAMETER TEST VEHICLE

The variable parameter test vehicle has been operated in excess of 800 hours. All systems operate as designed. The vehicle, when originally installed in the test station, was equipped with cooling straps on the cesium reservoir to permit low cesium reservoir temperature operation as required by the contract work statement (127°C). It was found that the straps created a thermal shunt around the reservoir heater and an accurate measurement of the true reservoir temperature could not be established. By removing the straps, the cesium reservoir temperature was accurately measured. The straps will be replaced after all high cesium pressure data have been obtained.

Preliminary electrical characteristics of the vehicle indicated the existence of a parasitic reservoir. This condition was remedied by proper heat shielding of the reservoir tubulation.

The variable spacing mechanism has proved capable of allowing accurate setting of the interelectrode spacing of the vehicle to within ±0.1 mil with a total travel in excess of 15 mils. The dial indicators reached a maximum temperature of 140°C with all auxiliary heaters on and a dc collector current of 80 amps for an emitter temperature of 1735°C. At this temperature, the spacing was accurately determined to within ±0.1 mil.

The guard ring equalizing load is performing satisfactorily. The guard ring potential is maintained within 10 millivolts of the collector potential and the collector current is maintained between 4.5 to 5 times that of the guard ring current. Figure 2-1 shows I-V characteristics for both the guard ring and the collector, indicating the current ratio between the two. The collector has a collecting area 4.9 times that of the collecting area on the face of the guard. These current ratios indicate successful action of the guard ring.

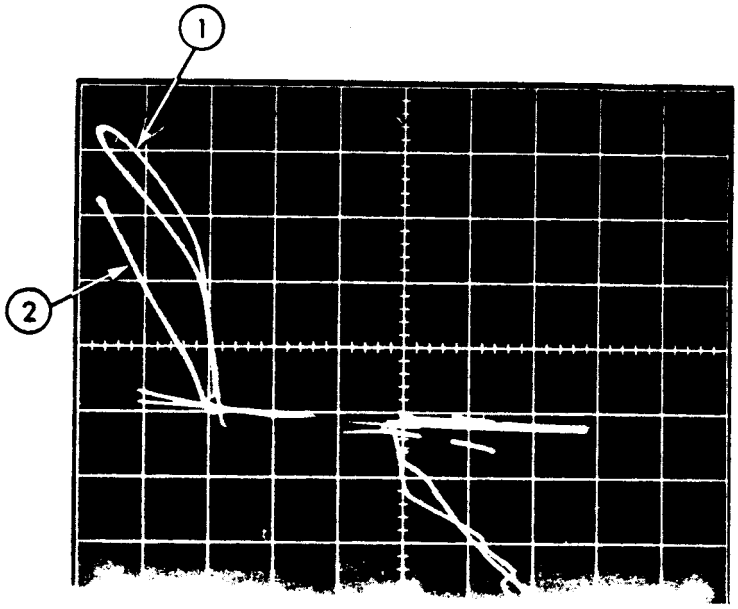

Curve 1: Collector Current
100 amps/div
0.5 volt/div

Curve 2: Guard Ring Current
40 amps/div
0.5 volt/div

FIG. 2-1 SAMPLE I-V CHARACTERISTIC FOR BOTH GUARD RING AND COLLECTOR

The principal purpose of the variable parameter test vehicle is to obtain precision thermionic converter optimization data. Subsection 2.1 discusses the determination of optimum collector, and reservoir temperatures to obtain maximum converter power output at 0.8 volt dc. In addition, current output variation as a function of interelectrode spacing at these specific dc voltages is presented. These data are essential for precision thermionic converter design. Data of a more basic nature are presented in Subsection 2.2 which discusses the variation of vehicle voltage output as a function of interelectrode spacing at a constant dc current. These data also provide the optimum spacing relationships for maximum power output as well as basic plasma parameter variations.

2.1 Converter Optimization Data

2.1.1 Measurement Technique

The converter optimization data near 0.8 volt output consisted of optimizing the dc current output of the vehicle as a function of spacing, cesium temperature, and collector temperature at a true emitter temperature of 1735°C true and at two voltage outputs of 0.8 volt and 0.7 volt measured at the current leads. The experimental procedure consisted of utilizing the electronic load to maintain a constant voltage output and setting a fixed collector temperature and a fixed spacing and varying the reservoir temperature until an absolute maximum in output current had been obtained. The cesium reservoir temperature was varied between 310°C and 350°C. At each fixed collector temperature, the spacing was varied between 0.002 and 0.005 inch. This procedure was repeated for collector root temperatures of 570°C, 596°C, 610°C, and 660°C. Collector root temperatures are quoted since the upper collector surface immersed thermocouple opened during the first few hours of vacuum outgassing. The precise matching collector surface temperature will be determined when the device is disassembled.

2.1.2 Measurement Results

The optimum parameters for maximum power output (15.44 watts/cm^2) at 0.8 volt are: collector root temperature 610°C, cesium reservoir temperature 331°C, and interelectrode spacing between 0.0032 and 0.0038 inch. The 0.8-volt data are shown in Figs. 2-2 through 2-5.

The data for 0.7-volt optimization have not been completed but some preliminary data are shown in Figs. 2-6 and 2-7. The complete optimum parameters will be determined during the next report period.

The maximum power variation at 0.8 volt as a function of spacing was measured with the collector root and reservoir temperature set at their optimum values. Keeping the voltage output constant at 0.8 volt by the electronic load and only varying spacing, the current output variation was determined. This is shown in Fig. 2-8. Of particular interest is the minimum power point observed at a spacing of 0.001 inch. As the spacing decreases further, the current (power) output increases again. This is the first time complete documentation of this behavior has been obtained in the emitter temperature region above 1300°C. The data show that only at spacings of less than 0.0003 inch will the power output exceed that available at a spacing of approximately 0.003 inch. The theoretical interpretation of this and following curves will be made in subsequent sections.

2.1.3 Discussion

From the standpoint of practical thermionic converter fabrication, the optimization of power output at a spacing of 0.0035 inch for the specified parameters increases the probability of long life operation at constant output, and reproducibility.

As indicated in Fig. 2-8, the only manner in which the power output may be increased from the practical maximum at 0.0035 inch is to reduce the spacing to less than 0.0003 inch. At this close

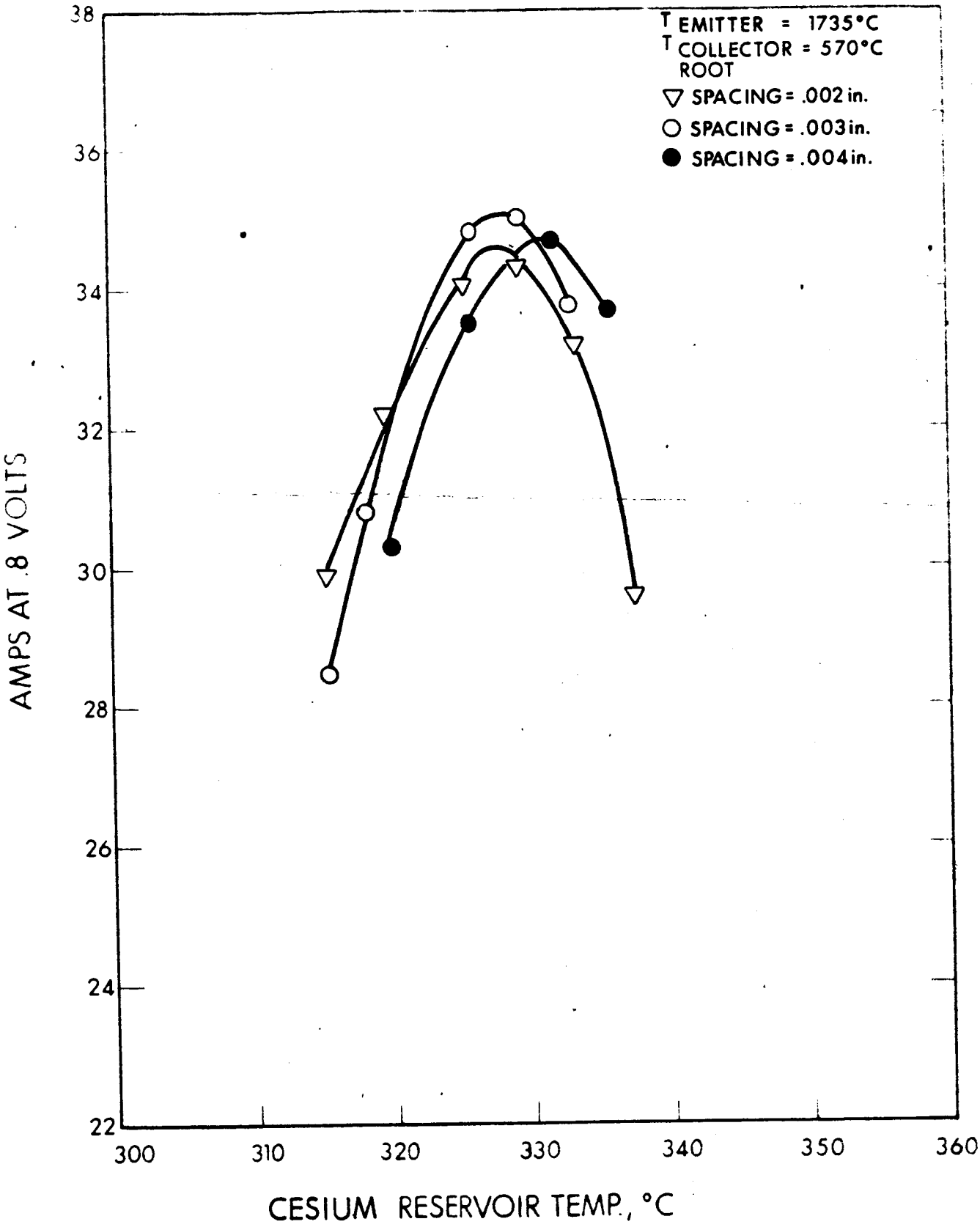

FIG. 2-2 RESERVOIR TEMPERATURE VERSUS CURRENT IN AMPERES WITH 0.002, 0.003, AND 0.004 INCH SPACING, $T_{COLLECTOR\ ROOT}$ = 570°C (all dc data points)

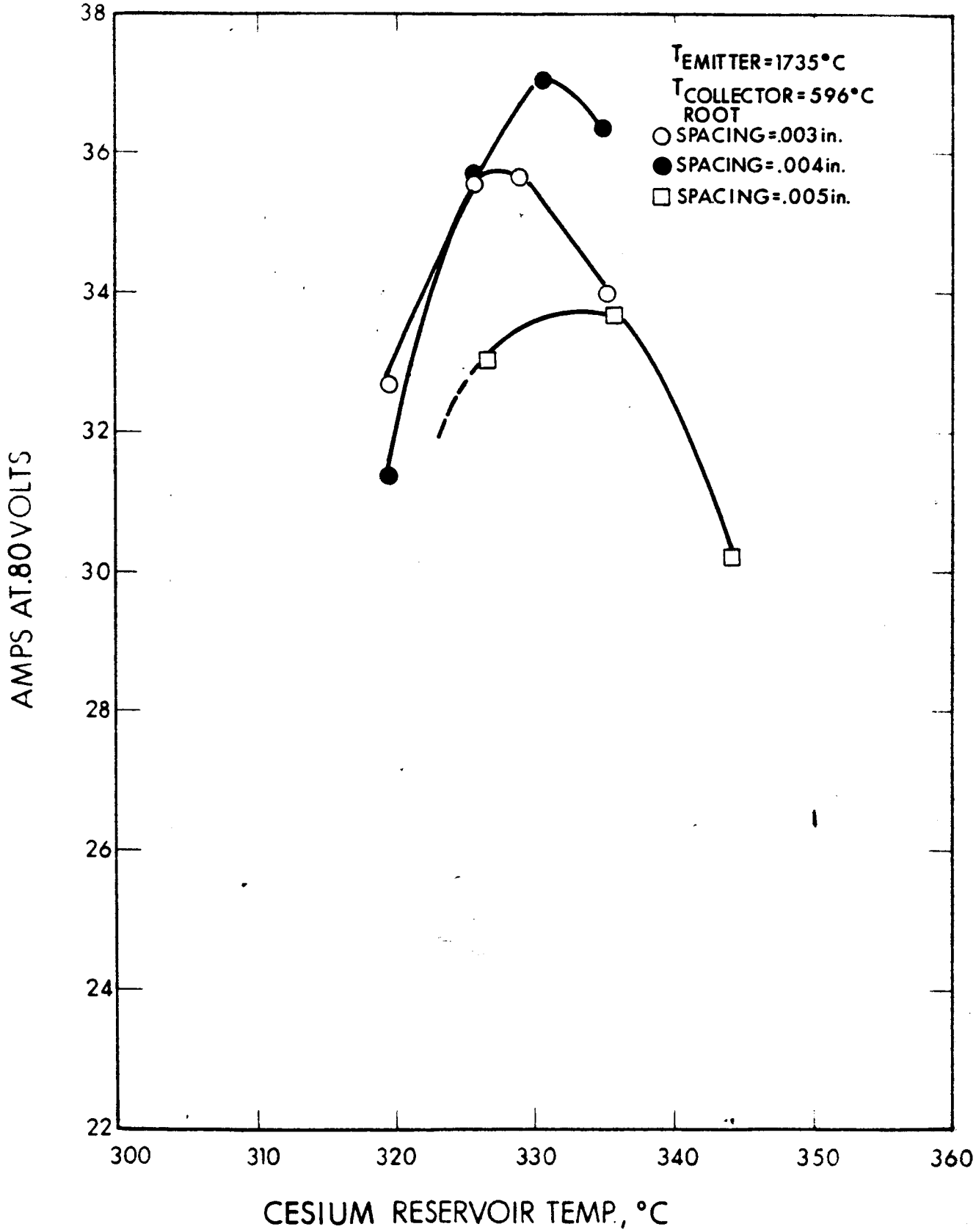

FIG. 2-3 RESERVOIR TEMPERATURE VERSUS CURRENT IN AMPERES WITH 0.003, 0.004, AND 0.005 INCH SPACING, $T_{COLLECTOR}$ = 596°C (all dc data points)

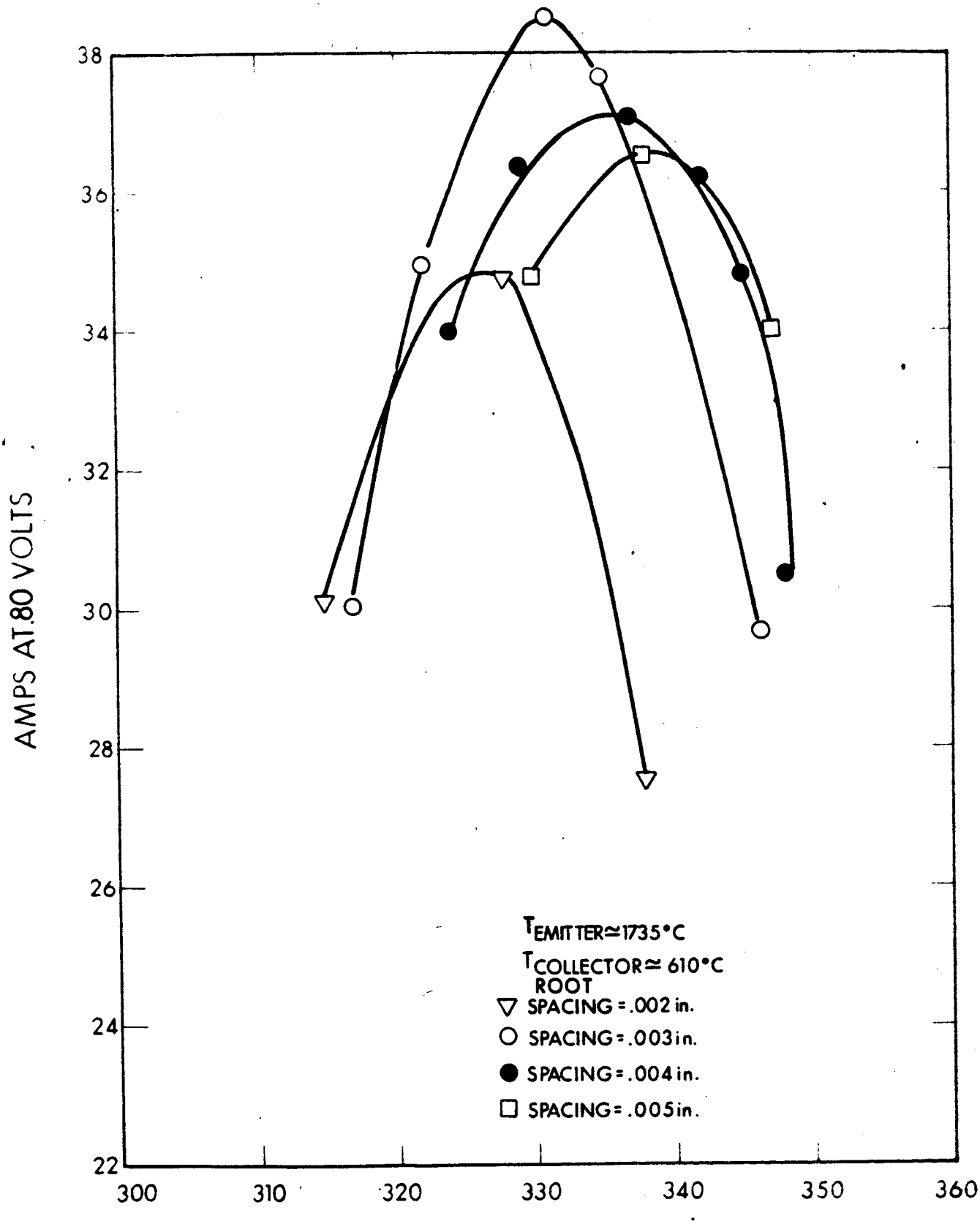

FIG. 2-4 RESERVOIR TEMPERATURE VERSUS CURRENT IN AMPERES WITH 0.002, 0.003, 0.004, and 0.005 INCH SPACING, $T_{COLLECTOR\ ROOT}$ = 610°C (all dc data points)

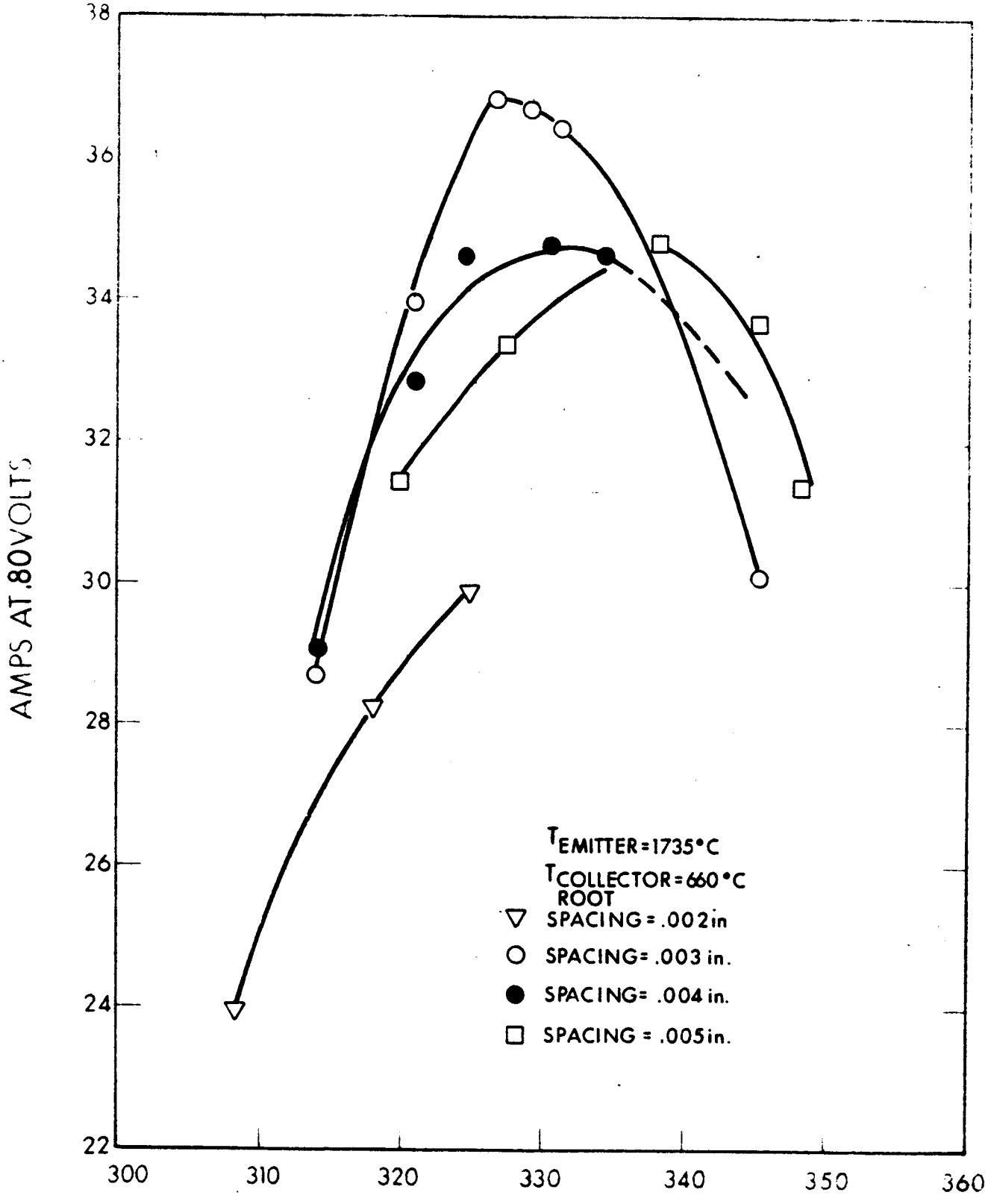

FIG. 2-5 RESERVOIR TEMPERATURE VERSUS CURRENT IN AMPERES WITH 0.002, 0.003, 0.004, AND 0.005 INCH SPACING, $T_{COLLECTOR\ ROOT}$ = 660°C (all dc data points).

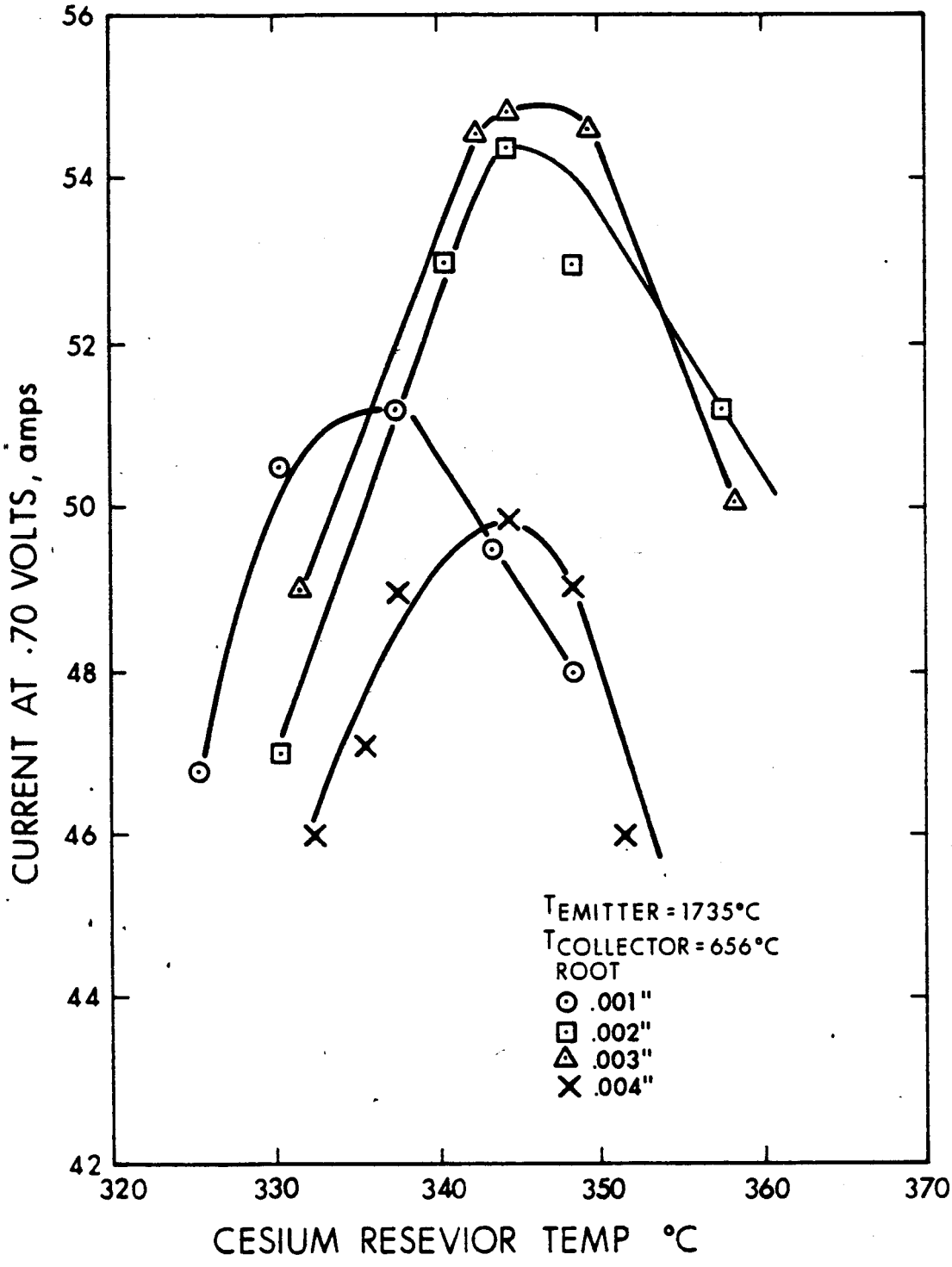

FIG. 2-6 0.7 VOLT CONVERTER OPTIMIZATION, $T_{COLLECTOR}$ = 656-665°C (all dc data points)
ROOT

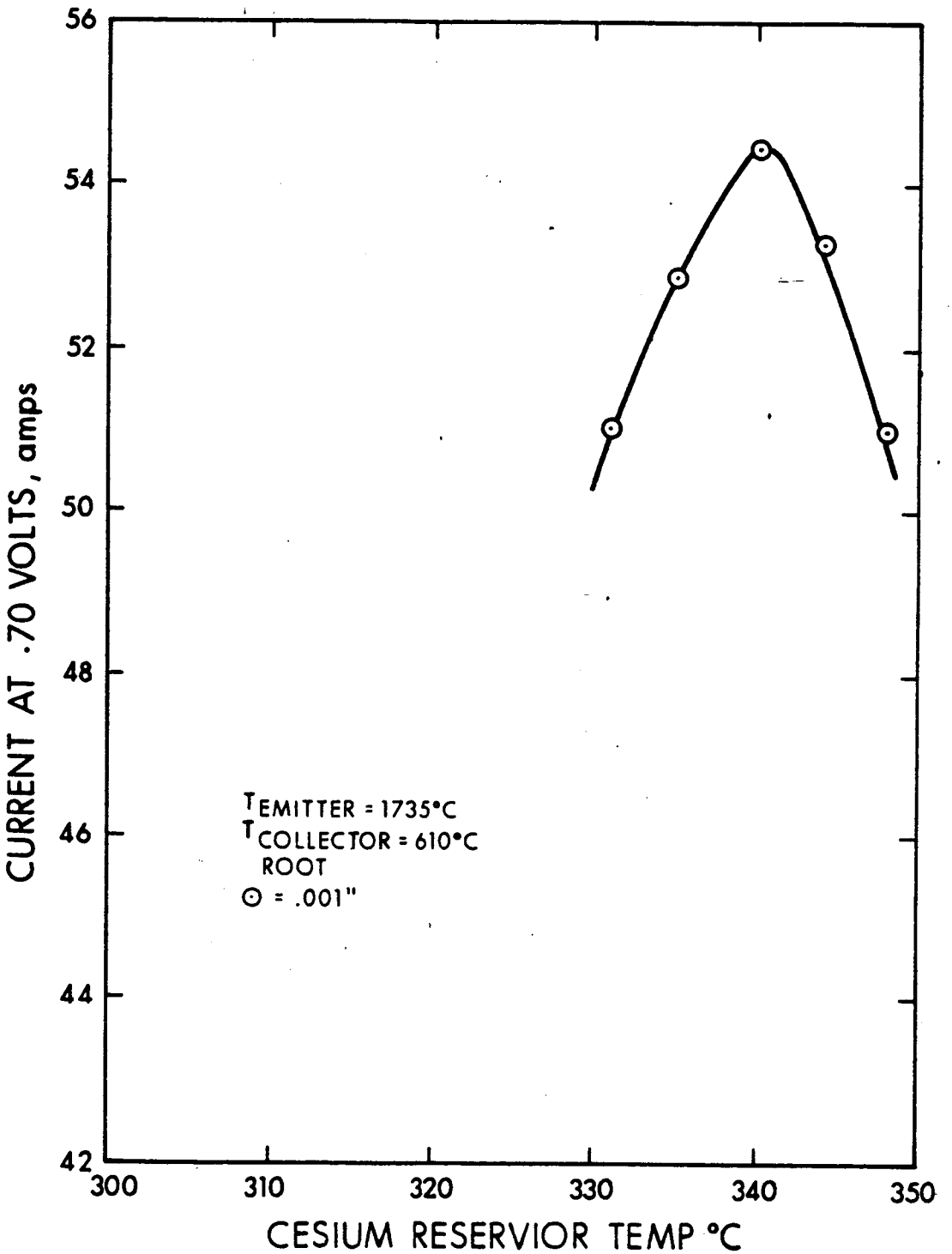

FIG. 2-7 0.7 VOLT CONVERTER OPTIMIZATION (all dc data points)

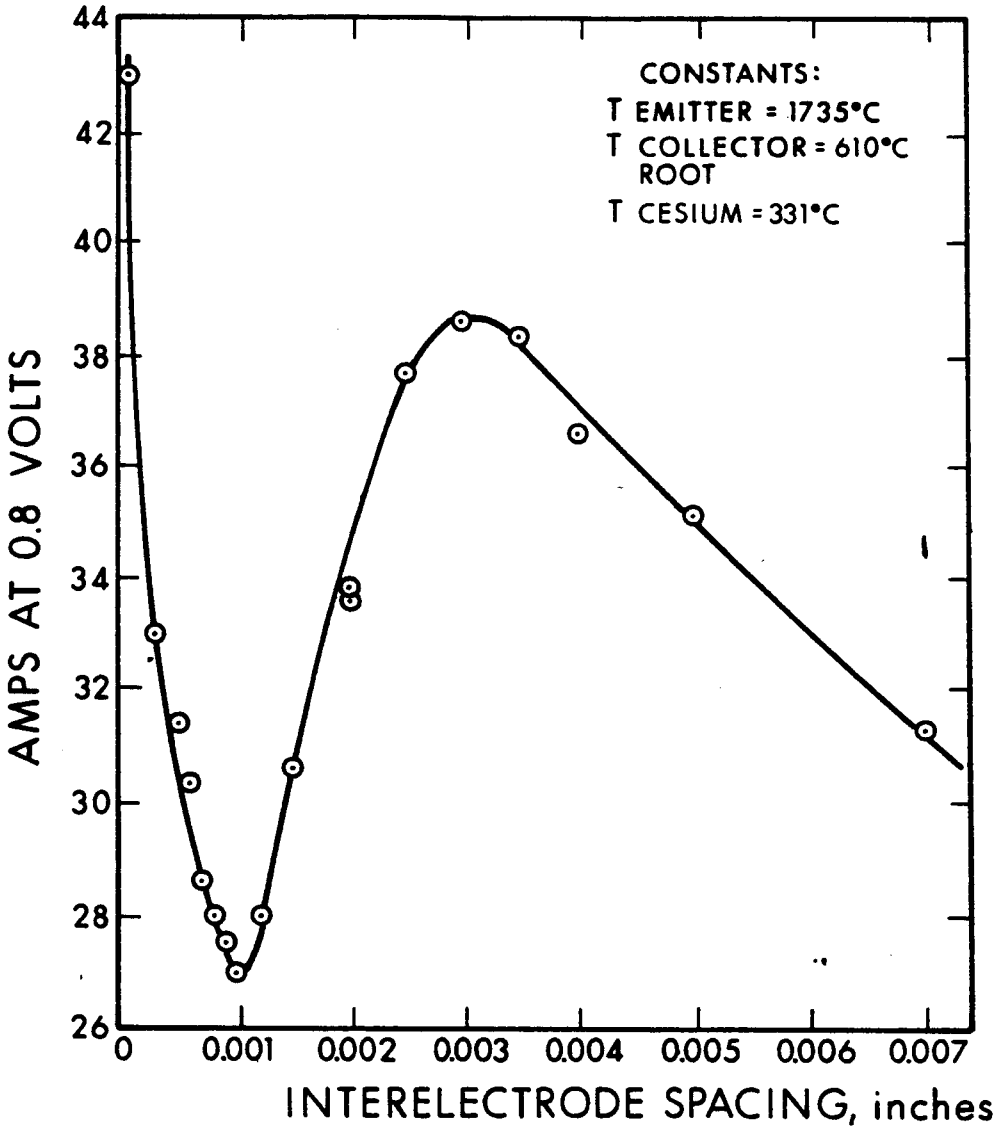

FIG. 2-8 INTERELECTRODE SPACING IN INCHES VERSUS CURRENT IN AMPERES AT 0.8 VOLT OUTPUT. COLLECTOR, EMITTER, AND CESIUM RESERVOIR CONSTANT TEMPERATURES (all dc data points)

spacing, the difficulty in fabrication and characteristic reproducibility is considerably increased as well as decreasing the reliability and usefulness of the device in some applications.

In apparent contradiction to these measurements is the accumulated experience of many thermionic converter suppliers, which essentially is that: the closer the spacing, the higher the power output. This statement is true, but requires qualification. This increase in power occurs only at the expense of voltage output. If a specific voltage output such as 0.8 volt is specified, the power output will vary as shown in Fig. 2-8.

2.2 Voltage-Spacing Relationships

2.2.1 Measurement Technique and Results

After establishing the variation of power output (at 0.8 volt output) with spacing shown in Fig. 2-8, it is desirable to relate the variation to the cesium plasma parameters. In order to achieve this, the power output is measured as a function of spacing at a constant dc current. The measured quantity is the voltage output variation with spacing at constant output. This variation of voltage with spacing at constant current is shown in Fig. 2-9. The advantage of this method is that all vehicle spacing problems due to differential expansion are eliminated due to the steady state vehicle temperature distribution.

Figure 2-9 is the voltage variation at a constant 38 amperes at the vehicle parameters for maximum power output of 0.8 volt, i.e., collector root temperature 610°C, cesium reservoir temperature 331°C. Figure 2-10 is a similar plot at a higher cesium pressure T_{cesium} = 350°C. The dc current is the same in Figs. 2-9 and 2-10, but the power output is lower for the higher reservoir temperatures. This is as expected, since the optimum power was determined to occur at T_{cesium} = 331°C.

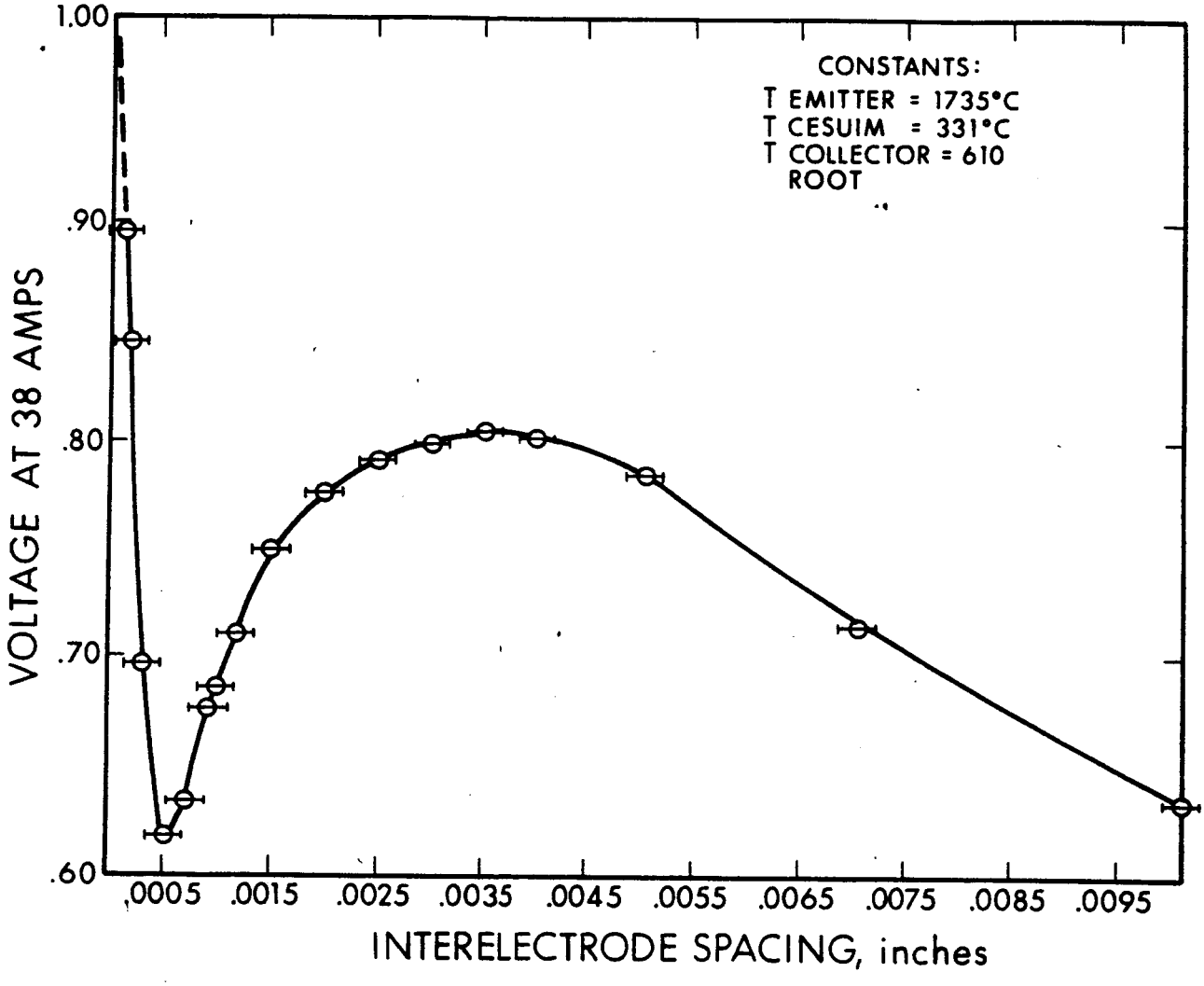

FIG. 2-9 INTERELECTRODE SPACING IN INCHES VERSUS VOLTAGE. EMITTER, COLLECTOR, AND CESIUM RESERVOIR TEMPERATURES CONSTANT (all dc data points)

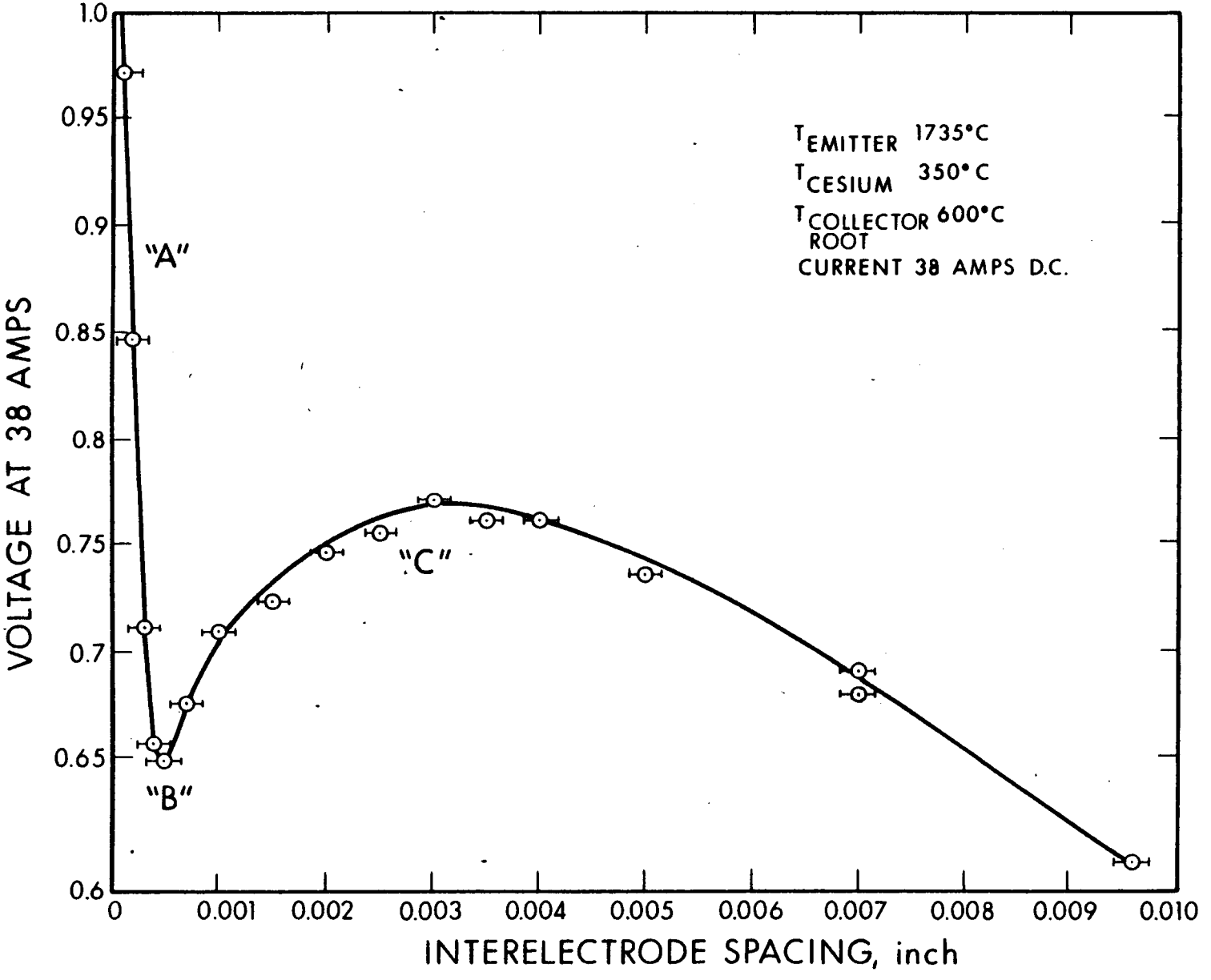

FIG. 2-10 VOLTAGE-SPACING RELATIONSHIP (all dc data points) FOR CONSTANT EMITTER, COLLECTOR, AND CESIUM RESERVOIR TEMPERATURES

Several interesting observations were made during accumulation of the experimental data: (1) at all spacings less than the minimum at 0.0005 inch the vehicle is operating in the space charge mode, (2) the minimum power point is a very unstable operating point due to the fact that at this spacing (0.0005 inch), the breakdown point coincides with the dc operating point and slight variations in temperature cause ignitions and extinguishing of the arc, and (3) the data were obtained by taking dc data points and then sweeping the vehicle with 60 cycles ac to take an oscilloscope I-V characteristic. Due to the increased collector heating and emitter cooling resulting from operation at the high current portion of the sweep, spacings less than 0.0003 inch cannot be maintained if the sweep is applied for more than approximately 30 seconds. High current sweep operation causes shorting of the vehicle at close spacings due to thermal expansion of the collector.

Figure 2-11 is a voltage-spacing curve for an emitter temperature of 1330°C and a dc current of 20 amperes.

2.2.2 Analysis and Interpretation

Utilizing Langmuir's equation to determine the cesium vapor pressure associated with a particular reservoir temperature:

$$\log_{10} P_{mm} = 11.0531 - 1.35 \log_{10} T_{^oK} - \frac{4041}{T_{^oK}} , \qquad (1)$$

the pd (mil-torr) for the relative maximum in Figs. 2-9 and 2-10 were determined. The results are shown in Table 2-I. The fundamental feature of the pd relations results from similarity relationships, that is, certain characteristics of a sustained discharge obey a similarity law relating dimensions and basic parameters. Therefore, for a discharge in identical gases and identical electrode materials,

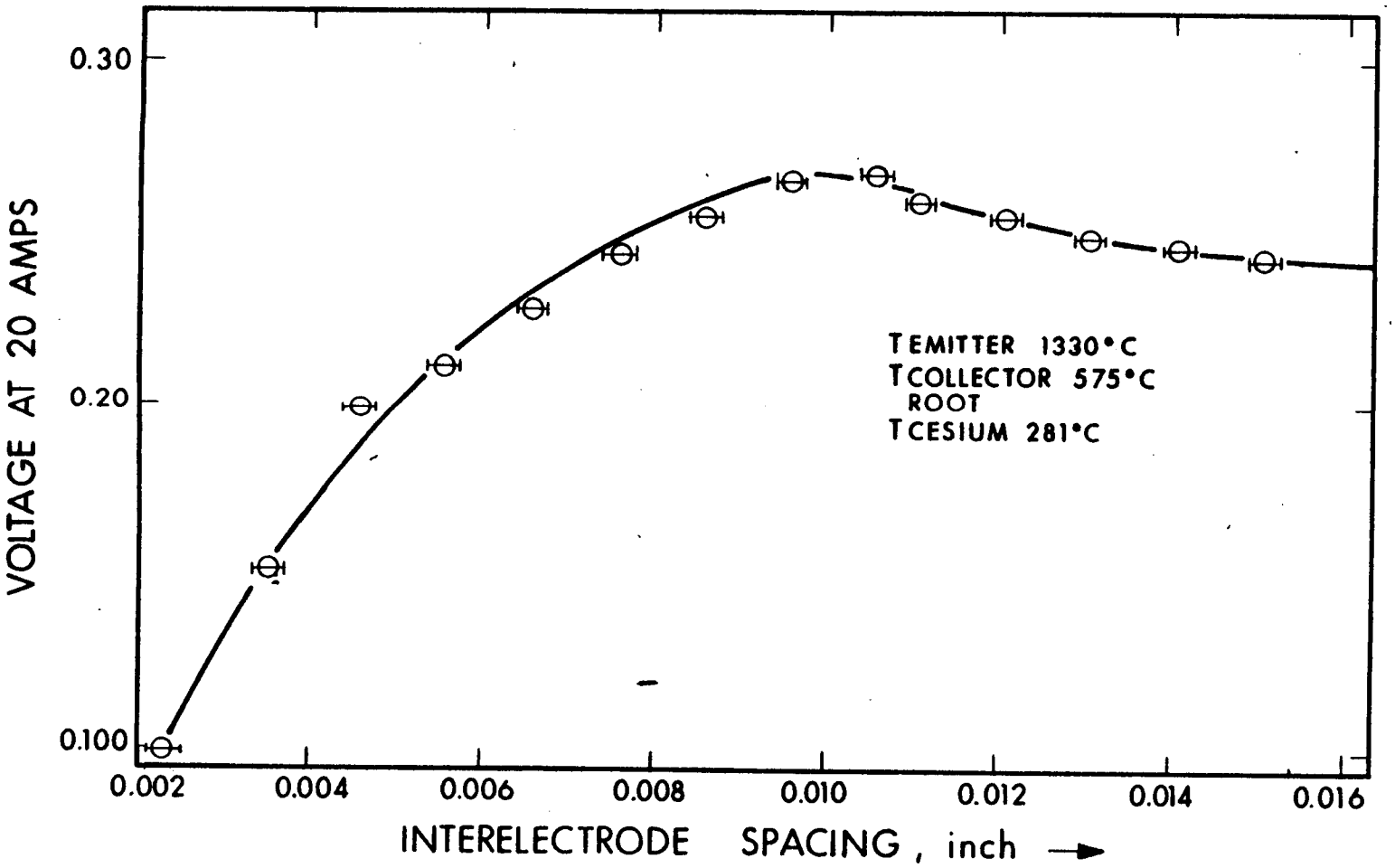

FIG. 2-11 INTERELECTRODE SPACING IN INCHES VERSUS VOLTAGE. EMITTER, COLLECTOR, AND CESIUM RESERVOIR TEMPERATURES ARE CONSTANT (all dc data points)

TABLE 2-I

T_{cesium} °C	P_{mm}	d (mil)	pd (mil-torr)
331	4.1 ±0.2	3.9	16.0 ±0.8
350	6.22 ±0.3	2.7	16.8 ±0.8

the vapor pressure, field intensities, and space potentials are directly related to the ratio of the spacings. Thus, as expected, the maximum power point of Figs. 2-9 and 2-10 occur at the same pressure-spacing product.

In all of these voltage-spacing measurements, the constant cesium reservoir temperature, collector root temperature, and emitter temperature along with constant current density results in a constant sheath thickness at the cathode and anode, constant plasma density, and constant plasma electron temperature. Therefore, the voltage output variation with spacing may be related to a voltage profile of the vehicle interelectrode space. This is not to say that the voltages in Fig. 2-9 can be interpreted as a direct measurement of the discharge potential. The voltage output of the test vehicle is related to the internal voltages by the following equation:

$$V_{out} = V_{cpd} + V_m - V_{cathode\ sheath} - V_{plasma} \pm V_{anode\ sheath} \qquad (2)$$

where

V_{cpd} = contact potential difference between the cathode and anode

V_m = space charge minimum voltage, i.e., if a double sheath exists at the cathode, V_m = voltage barrier necessary for an electron to overcome proceeding from the cathode surface to the accelerating portion of the sheath

$V_{\text{cathode sheath}}$ = potential drop from the voltage minimum to the plasma

V_{plasma} = potential drop in the plasma

$V_{\text{anode sheath}}$ = value of the accelerating or retarding voltage at the collector

$V_{\text{anode sheath}}$ may be zero under certain conditions of electrode geometry, anode temperature, and spacing. Thus, the variation of output voltage with spacing is a summation of all the spacing dependent terms of Eq. 2.

Figure 2-10 has three points of interest designated on the curve for the voltage variation with spacing at a cesium temperature of 350°C. I-V characteristics for each of the points of interest are shown in Fig. 2-12. Point "A" shows the characteristic at an interelectrode spacing of 0.0002 inch; the dc point of 38 amps current is plainly visible on the characteristic. The breakdown spike can be observed at the top of the photograph occurring at approximately 60 amps and 0.5 volt. It is apparent from this characteristic that the vehicle for a spacing of 0.0002 inch and at the dc operating point is operating in the space charge limited mode. Figure 2-13 shows the potential distribution in the interelectrode space at the specific points on the voltage spacing curve. Again, point "A" indicates the classical double-diode space charge distribution. Point "B" is at the minimum of the voltage-spacing curve. Figures 2-12 and 2-13 show the I-V characteristic and potential distribution at this point of operation. As can be seen in Fig. 2-12, the dc operating point for point "B" occurs directly at the breakdown point. This operating point is very unstable since the constant current point can occur at two different voltages. Compared to point "A", the voltage output has decreased to allow for the accelerating potential distribution for electrons into the anode. A plasma has not developed yet, but as this potential approaches the first excitation potential for cesium, the ionization mechanisms can be optimized. This process continues until point "C" is reached. At

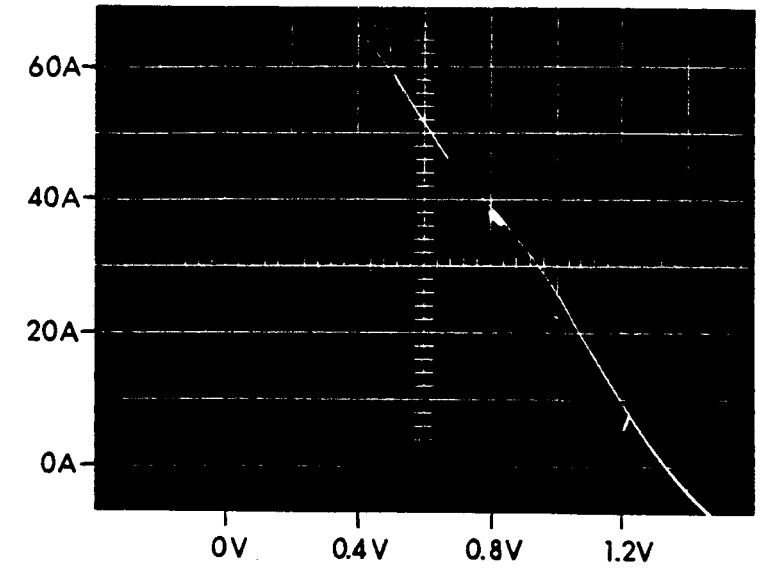

Pt. "A"

T_e = 1735°C

T_{Cs} = 348°C

Spacing = 0.2 mil

I_{dc} = 38 amps

$T_{coll\ root}$ = 300°C

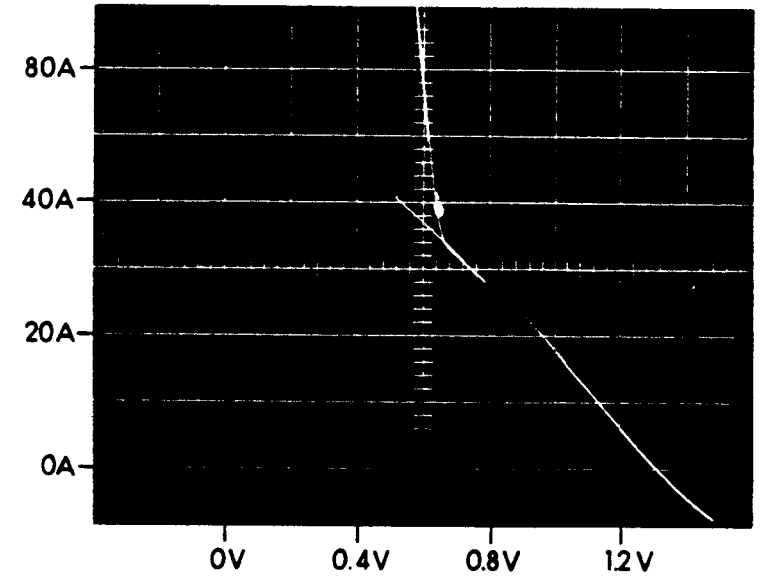

Pt. "B"

T_e = 1735°C

T_{Cs} = 350°C

Spacing = 0.5 mil

I_{dc} = 38 amps

$T_{coll\ root}$ = 300°C

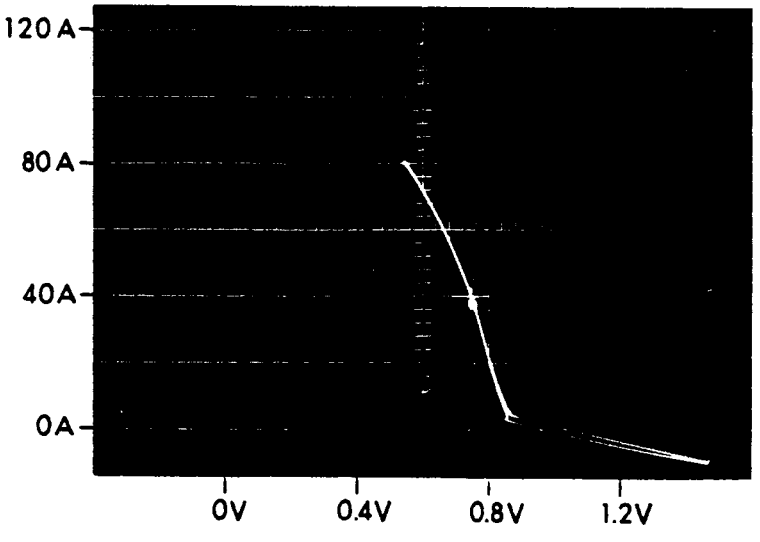

Pt. "C"

T_e = 1735°C

T_{Cs} = 348°C

Spacing = 3.5 mils

I_{dc} = 38 amps

$T_{coll\ root}$ = 300°C

FIG. 2-12 I-V CHARACTERISTICS FOR THE OPERATING REGIONS OF SPACE-CHARGE LIMITED, INCIPIENT BREAKDOWN, AND FULLY DEVELOPED PLASMA (Ref. Fig. 2-10)

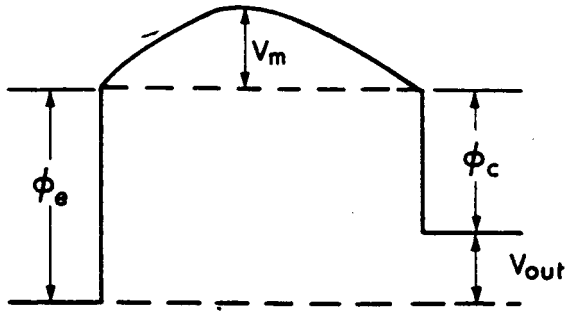

POINT "A"

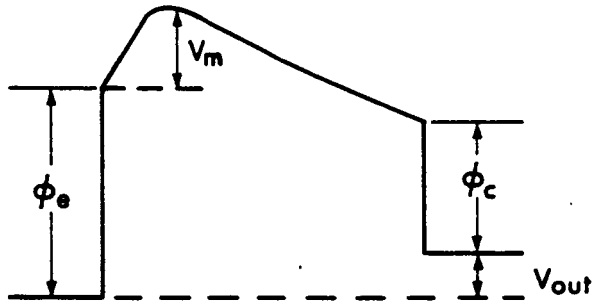

POINT "B".

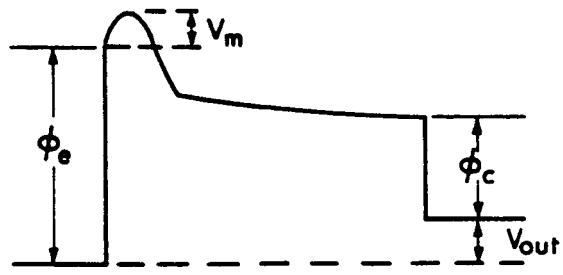

POINT "C"

FIG. 2-13 POTENTIAL DISTRIBUTION DIAGRAM FOR SPACE CHARGE, INCIPIENT BREAKDOWN AND FULLY DEVELOPED PLASMA AT THE dc POINTS "A", "B", "C"

this point, a fully-developed plasma exists as typified by the potential diagram of point "C" in Fig. 2-13. In all of the potential diagrams of Fig. 2-13, the potential is shown matched to the anode. Since, depending on the geometry and anode temperature, the anode sheath can either be accelerating, decelerating, or matched to the anode for simplicity, the diagrams were constructed as shown.

To further clarify the gas discharge nature of the cesium thermionic converter, a preliminary analysis was performed on the space charge region of the voltage-spacing curve of Fig. 2-10. Using both the Childs-Langmuir space charge equation and the collision dominated space charge equation, dV/dx was calculated:

$$J = \frac{1}{9\pi}\sqrt{\frac{2e}{m}}\frac{V^{3/2}}{d^2} \qquad \text{Childs-Langmuir} \qquad (3)$$

$$J = \frac{9}{8}\epsilon_o \frac{\Lambda^2 \nu}{T_{electron}}\frac{V^2}{x^3} \qquad \text{Collision dominated} \qquad (4)$$

where

Λ = electron-atom mean free path

ν = electron-atom collision frequency

$T_{electron}$ = electron temperature.

The transition from the classical space charge limited mode and the plasma dominated region indicated in Fig. 2-10 results from the increase in the space charge current (86 percent) produced by ion neutralization and the increased contribution of the collision dominated space charge current given by Eq. 4. A complete analysis of this situation will be provided in the final report. dV/dx was then evaluated at point "A" where X = 0.0002 inch and J is a constant 19 amperes/cm^2. The results are shown in Table 2-II.

TABLE 2-II

dV/dX at 0.0002 inch		
Eq. 3	Eq. 4	Experimental
431 volts/cm	22.6 volts/cm	512 volts/cm

Table 2-II indicates that within the accuracy of experimental determination, the Childs-Langmuir law applies to region "A" of Fig. 2-10 and for these short spacings the vehicle is definitely operating in the classical space charge limited mode.

A point-by-point differentiation of the curve in Fig. 2-10 is shown in Fig. 2-14. This is not a plot of the internal field intensity since the plot is of dV_{out}/dx. Differentiating Eq. 1 results in:

$$\frac{dV_{out}}{dx} = \frac{dV_{cathode\ sheath}}{dx} - \frac{dV_{plasma}}{dx} + \frac{dV_{anode\ sheath}}{dx} \qquad (5)$$

Therefore, Fig. 2-14 represents the contributions of several spacing dependent terms in the voltage output equation. The shape of the curve is similar to the field intensity distribution of a gas discharge, but further analysis will be required to completely pin-point the regions of influence of each of the voltage output equation terms. One observation can be made at the present time. The constant dV_{out}/dx beyond point "C" seems indicative of the formation of a positive column in the plasma of a thermionic converter for interelectrode spacings greater than 0.0035 inch and the general device parameters stated.

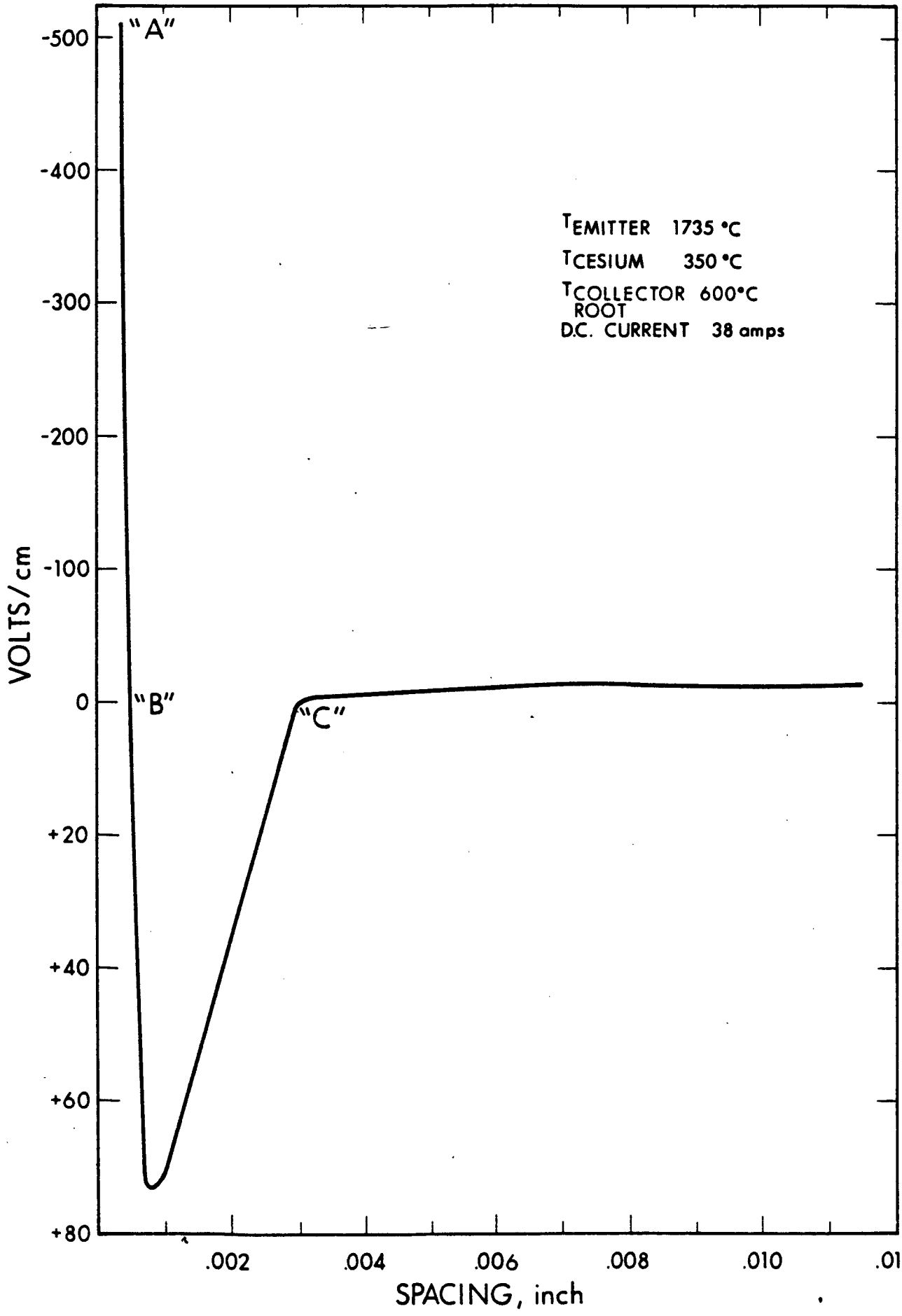

FIG. 2-14 FIRST DERIVATIVE OF VOLTAGE-SPACING CURVE

2.3 Cesiated Work Function Measurements

2.3.1 Measurement Techniques

In all of the reported measurements, the volt-ampere characteristics are obtained by the combined dc and ac method. This method is utilized since it traces an instantaneous characteristic at fixed parameter temperatures. The dc operating point is usually set by the electronic load. The sweep transformer then sweeps out a given portion of the complete I-V characteristic around this dc point. Collected current is determined by measuring the voltage drop across a calibrated, 0.1-percent-accurate shunt and displayed on the y-axis of an X-Y scope. Applied voltage or generated voltage is measured directly across the vehicle leads and displayed on the x-axis of the oscilloscope. In order to accurately determine saturated emission, it is necessary to sweep the arc voltage as much as 2 volts into the applied voltage quadrant. Since the diodes in the electronic load, discussed in previous reports, cannot hold-off more than 0.5 volts, the electronic load was replaced by a manual load across the vehicle and a low inductance, low impedance, secondary step-down transformer employed as a sweep source. The saturated emission is defined as the intersection of the extrapolated Schottky slope and slope of the plasma region. The large applied voltage is necessary to define the Schottky slope. Figure 2-15 consists of three volt-ampere characteristics with an applied voltage of between 1.5 and 2.0 volts. To assure that a true saturated emission was being measured, the emission was measured at three interelectrode spacings: 0.001, 0.003, and 0.006 inch. The characteristics show that the measured saturated emission was constant within ±5 percent while the spacing varied by a factor of six.

Exact determination of temperature is a very important part of accurate electron emission measurements. For all temperature determinations, other than the emitter and collector, calibrated

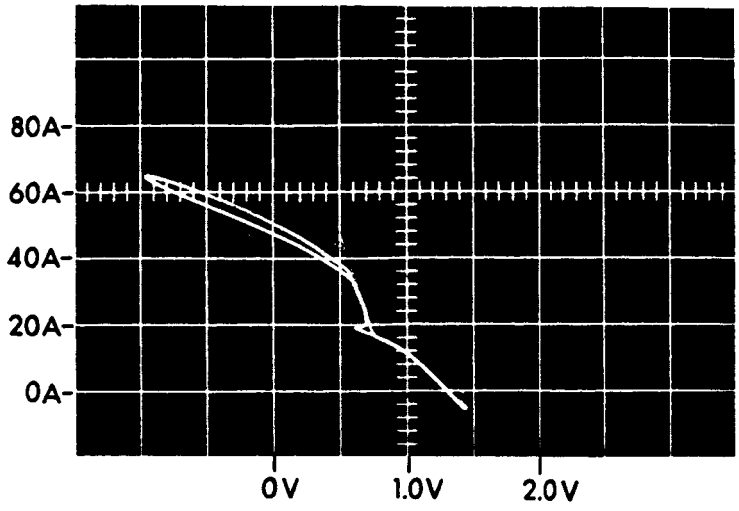

T_e = 1700°C
T_{Cs} = 316°C
Spacing = 1 mil
Saturated emission = 42 amps

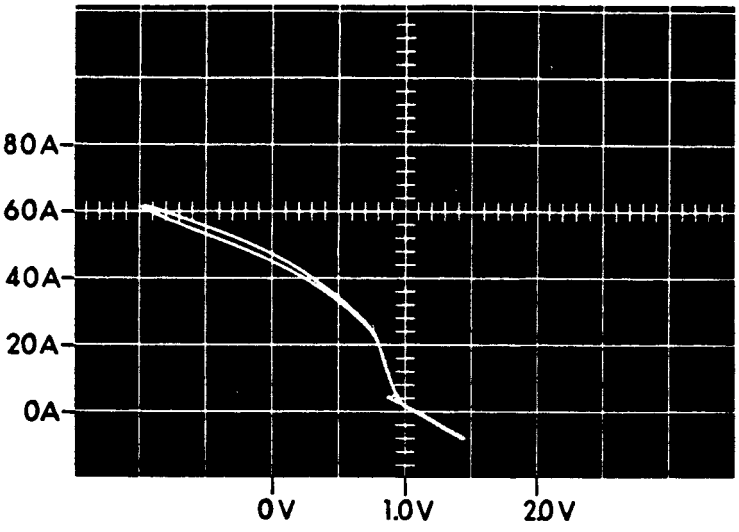

T_e = 1700°C
T_{Cs} = 316°C
Spacing = 3 mils
Saturated emission = 39 amps

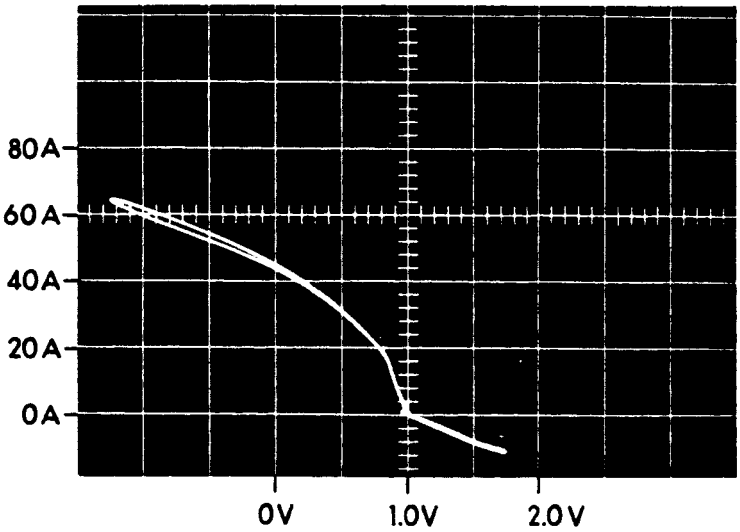

T_e = 1700°C
T_{Cs} = 315°C
Spacing = 6 mils
Saturated emission = 39.5 amps

FIG. 2-15 I-V CHARACTERISTICS SHOWING THAT SATURATED ELECTRON EMISSION IS INDEPENDENT OF SPACING

chromel-alumel thermocouples traceable to the National Bureau of Standards were used. The emission measurements were conducted over the emitter temperature range between 1000°K and 2000°K. The temperature for the higher portion of the emitter range (above 1200°C) can be determined very accurately by comparing the color of 8-to-1 blackbody hole in the emitter with a micro-optical pyrometer. Below 1200°C, optical temperature measuring methods require large corrections due to radiation reflections and emissivity changes. Therefore, thermocouples are required to measure the temperature ranges below 1200°C. Tungsten 5 percent rhenium, tungsten 26 percent rhenium thermocouples were attached to the emitter by tantalum pads. These thermocouples were calibrated by platinum rhodium couples in the lower range and blackbody holes in the higher range to give the saturated emission data continuity over the complete temperature range. Figure 2-16 shows the thermocouple calibration.

2.3.2 Cesiated Emitter Work Function Results

Figure 2-17 is a plot of the saturated electron emission from polycrystalline rhenium. There are two significant results to be obtained from this figure: the electron current density and the minimum work function. The electron density measured from the polycrystalline rhenium emitter is a factor of two higher than {110} single crystal tungsten emission (Ref. 1) measured for approximately the same cesium reservoir temperatures (arrival rate), and a factor of ten higher than the cesiated electron emission measured from polycrystalline molybdenum (Ref. 2). The minimum work function for the polycrystalline rhenium is converging to a value of approximately 1.45 volts. This work function is between 0.1 and 0.15 volt less than the minimum work function reported for polycrystalline tantalum, polycrystalline molybdenum (Ref. 2) and {110} single crystal tungsten (Ref. 1).

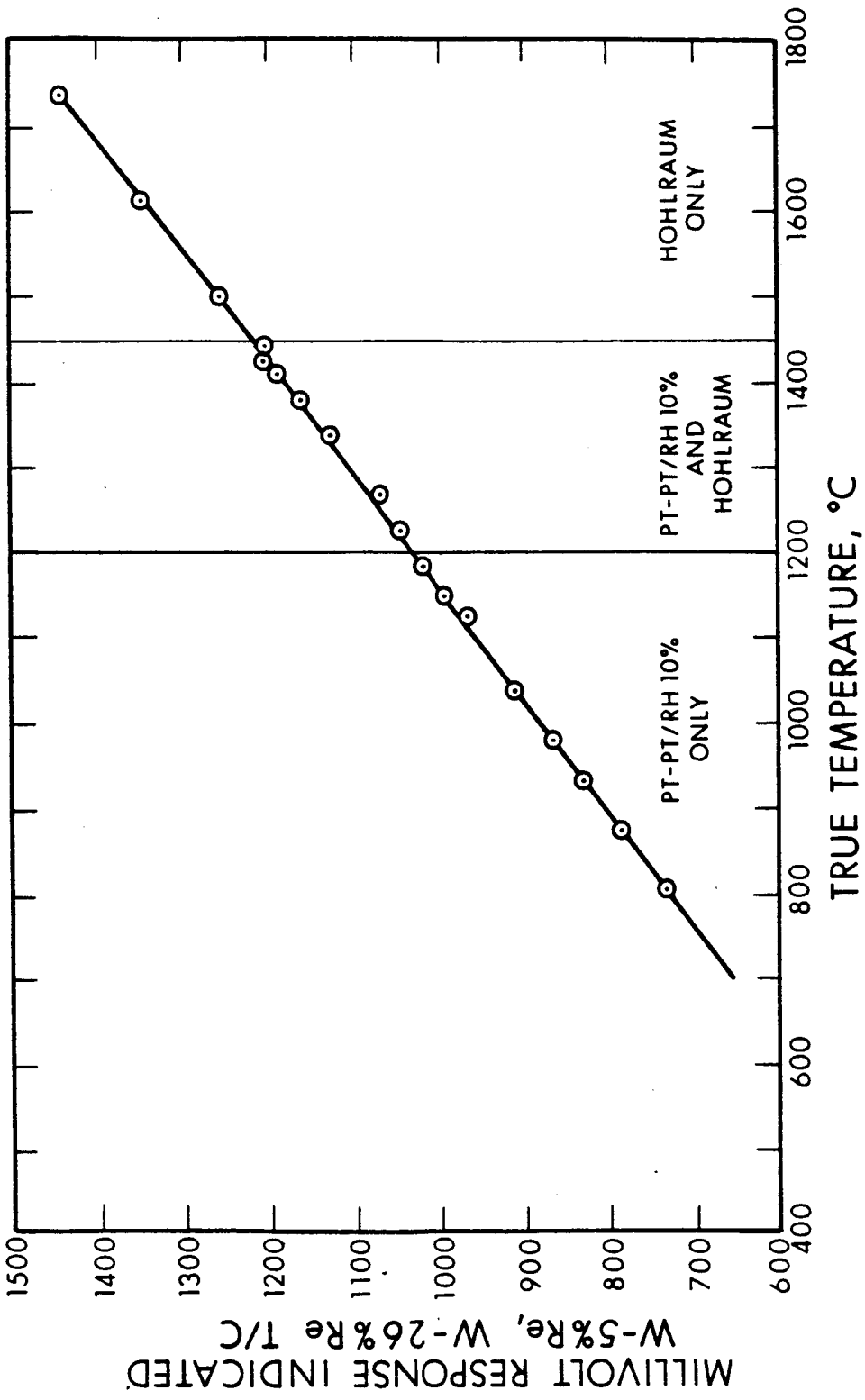

FIG. 2-16 THERMOCOUPLE CALIBRATION DATA

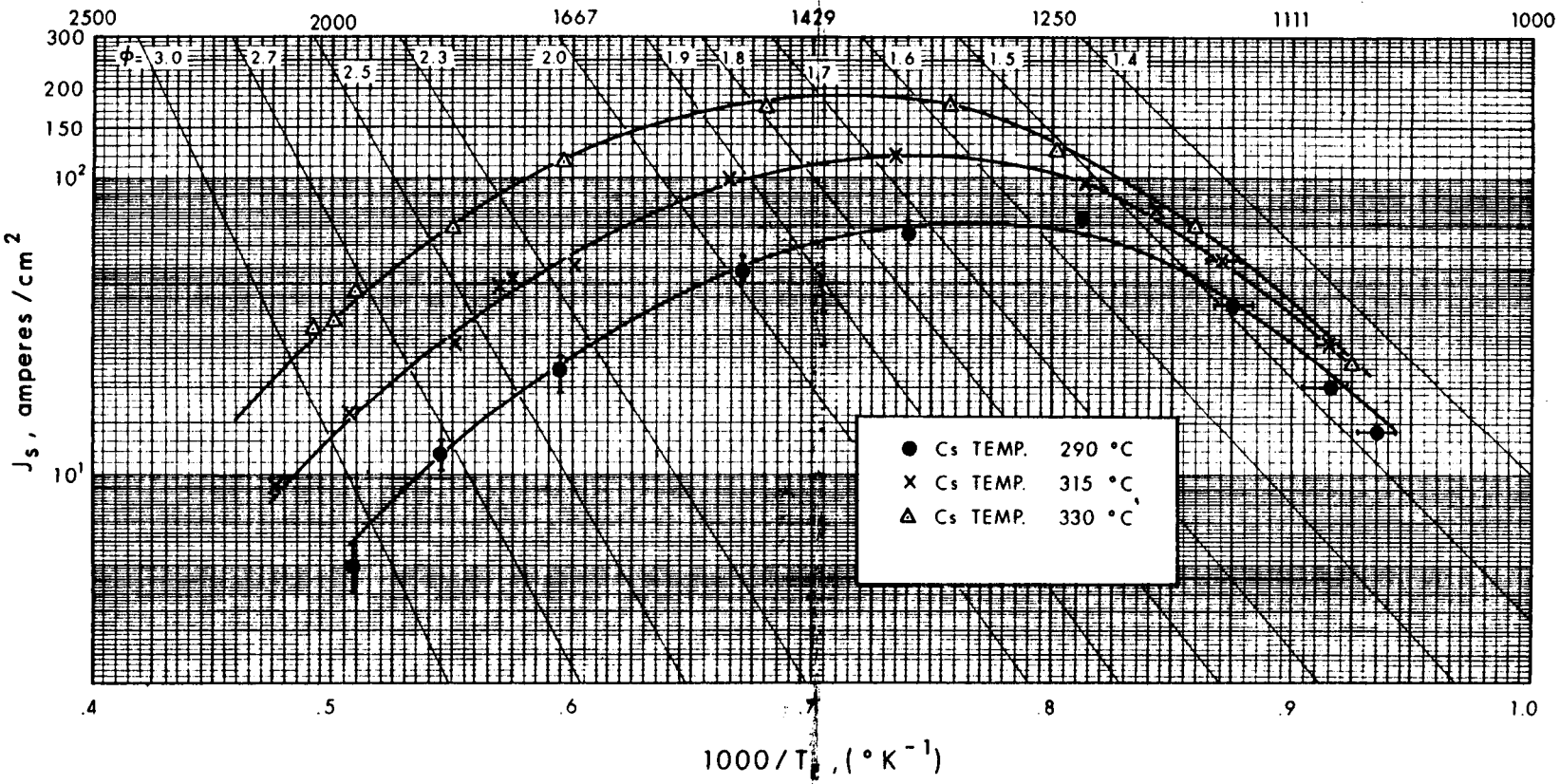

F[illegible] 2-17 S[illegible]TED ELECTRON EMISSION FROM POLYCRYSTALLINE RHENIUM

The importance and value of these data is that they were obtained in a system and manner directly related to operational thermionic energy converters. Therefore, converter performance can be accurately predicted from the data obtained from this vehicle.

2.3.3 Collector Work Function Results

To determine collector surface work functions, the saturated emission from the collector must be measured. This is obtained by sweeping the volt-ampere characteristic beyond open circuit voltage. This is in effect reversing the potential distribution within the interelectrode space, allowing the collector to act as an emitter. Figure 2-18 shows two oscilloscope sweeps for two different sets of parameters. In these photographs the forward saturated emission is obtained in the positive applied voltage quadrant and the reverse saturated emission (from the collector) is obtained in the negative applied voltage quadrant. Knowing the collector surface temperature, the saturated emission can be plotted versus temperature, in the same manner as the emitter data were presented. Since the collector surface thermocouple was inoperative, no accurate determination of collector work function could be made during these tests. An approximate collector work function can be determined by making various approximations. The first quarterly report discussed the thermal conduction of a mock collector under various heat input and dissipation conditions. If L/A corrections are made to correlate those data with the existing collector geometry on the variable parameter vehicle, the temperature drop down the collector barrel should be no greater than $100^{\circ}C$ for a thermal input of 265 watts/cm^2 and no less than $40^{\circ}C$ for a thermal input to the collector surface of 150 watts/cm^2. Therefore, for a collector root temperature of $727^{\circ}C$ and a collector saturated emission of 42.5 A/cm^2 as shown in Fig. 2-18, a collector work function between 1.42 and 1.34 volts is obtained. For the second case in Fig. 2-18, the work function would lie between 1.45 and 1.36 volts. This correlates well, considering the circumstances, with the emitter saturated emission data presented in Fig. 2-17.

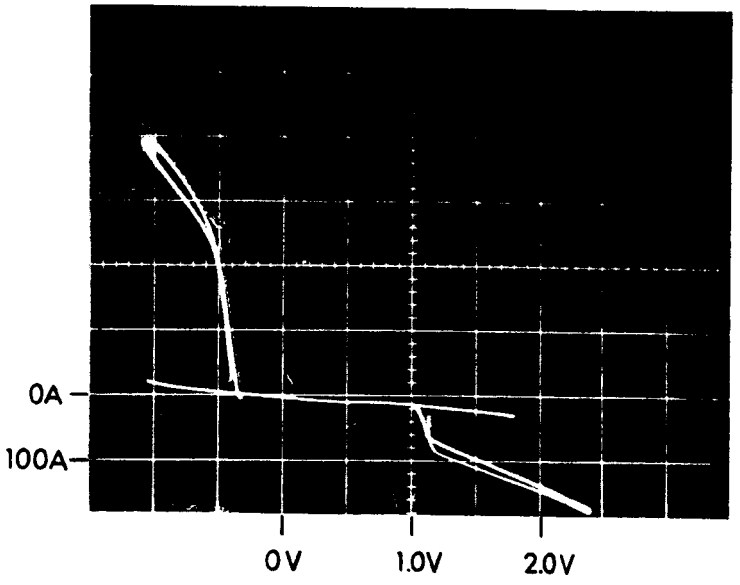

$T_{coll\ root}$ = 727°C

T_{cesium} = 315°C

Collector saturated emission = 85 amps

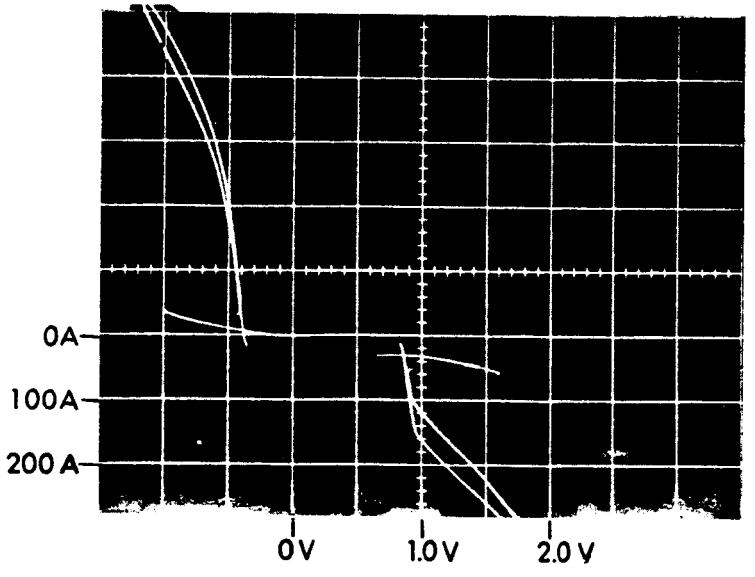

$T_{coll\ root}$ = 783°C

T_{cesium} = 330°C

Collector saturated emission = 155 amps

FIG. 2-18 SATURATED EMISSION MEASURED FROM COLLECTOR SURFACE

2.4 Bare Work Function Measurements

Bare work function, or more properly, low cesium coverage (i.e., $\theta \leq 0.01$), measurements were taken from the rhenium emitter. The saturated electron emission was measured over the emitter temperature range from 1973°K to 2133°K at a reservoir temperature of 122°C which was the minimum achievable. The work function was computed by way of the Richardson-Dushman equation assuming a pre-exponential A value of 120 amps/cm^2 - °K^2. The work function values are indicative of the upper portion or high temperature end of the Langmuir "S" curve ranging in value from 4.45 volts to 4.75 volts, the latter value representing a close approach to the condition of no cesium coverage on the emitter surface.

2.4.1 Measurement Techniques and Results

There are two problem areas in obtaining electron emission measurements where current densities are low and emitter temperatures high. Low current density measurements are difficult to make since leakage paths are available across cesium-coated ceramics. To eliminate this leakage source, a dc null circuit was employed which voided current leakage over the collector and guard ring insulators. The schematic for this null circuit is shown in Fig. 2-19. All instruments used in the circuit were Sensitive Research meters certified at 0.1 percent accuracy. A point-by-point dc measurement of the test vehicle I-V output was plotted utilizing the null circuit. Three such curves are shown in Fig. 2-20 where each point on the curve is a dc, steady-state value read from high accuracy meters.

The second problem in obtaining emission data is accurate temperature measurement of the emitting surface. Identical to all emitter temperature measurements in excess of 1100°C reported from the test vehicle, the temperature was determined by directly viewing an 8:1 depth-to-diameter hohlraum with a micro-optical pyrometer which is periodically calibrated against a NBS standard lamp.

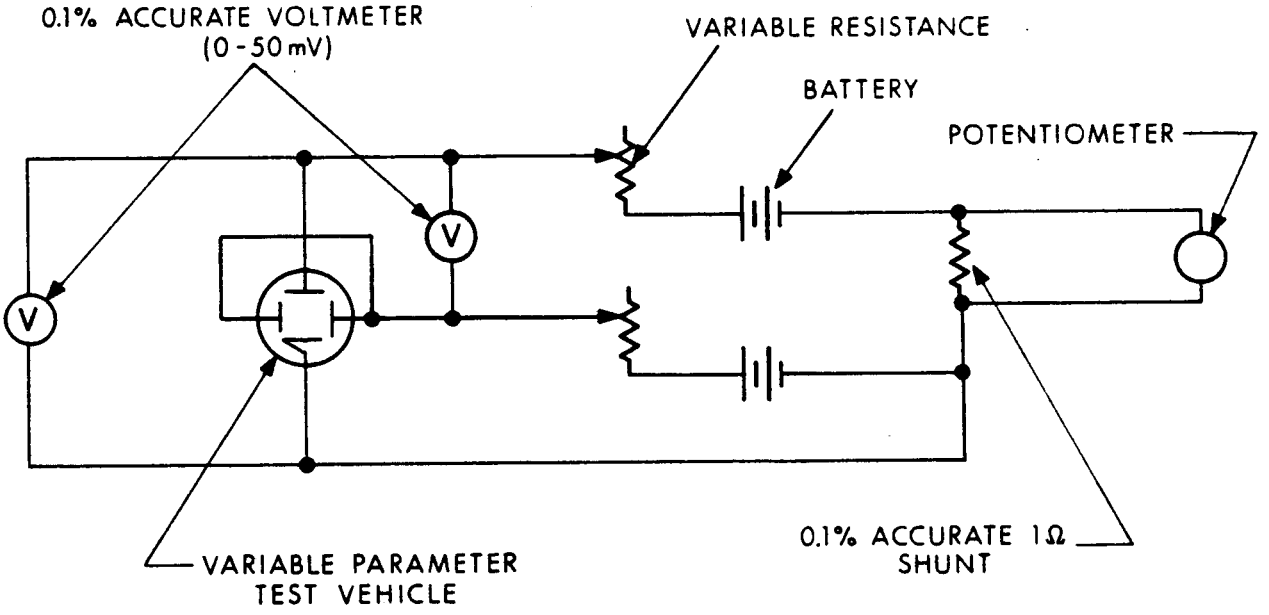

FIG. 2-19 CIRCUIT FOR BARE-WORK FUNCTION MEASUREMENTS

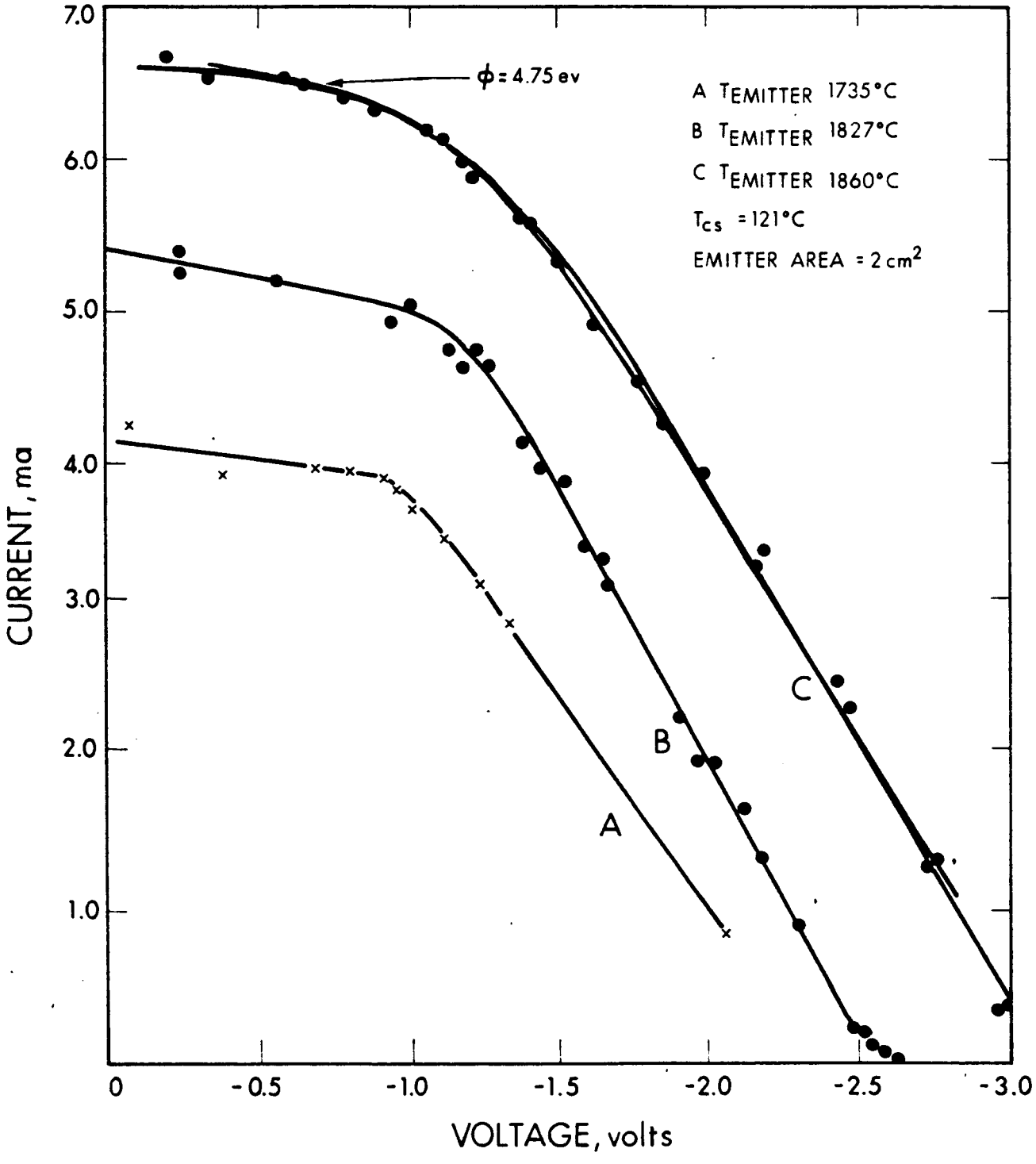

FIG. 2-20 I-V CURVES (dc points) FOR BARE-WORK MEASUREMENTS (all dc data points)

For the high emitter temperatures (i.e., 2000°K), the normal transmission loss through the bell jar increases. It was therefore necessary to correct the observed temperature by an additional 8°C to 13°C depending on the temperature.

2.4.2 Discussion of Results

Table 2-III summarizes the measurements taken from the emitter at the conditions described. The bottom of the "S" curve is evident from the work function change of only 0.02 volts over a 100°C increase in emitter temperature. Emitter temperatures higher than 2133°C are desirable to complete the picture of a noncesium-covered value of 4.75 volts; however, higher emitter temperatures may alter the surface structure of the emitter and render the previous pd data and cesiated emission measurements nonreproducible.

TABLE 2-III

SUMMARY OF BARE WORK FUNCTION MEASUREMENTS

J_S Amp/cm^2 x 10^{-3}	T (°K)	ϕ (Volts) A = 120 amps/cm^2 - °K^2
1.8	1973	4.45
1.85	2008	4.53
2.42	2100	4.55
3.25	2133	4.75

NOTE: Data taken at a constant cesium reservoir temperature of 122°C.

Curve B from Fig. 2-20 was plotted on semilog paper to analyze the Boltzmann slope of the I-V curve. Except at the bottom-most portion of the curve where some exponential behavior is apparent, there does not appear to be a true retarding field portion of the curve. This lack of linearity is probably caused by the presence of cesium atoms in the interelectrode spacing giving rise to collisions. As noted previously, it was not possible to easily lower the reservoir temperature below 122°C.

2.5 Cesium Conduction Measurements and Results

2.5.1 Measurement Techniques

To measure the heat transfer from a thermionic emitter due to cesium vapor conduction requires the detection of small changes in heat input to the emitter. Therefore, it is desirable to reduce or completely omit electron emission from the emitter during the course of these measurements since the heat transfer associated with electron evaporation from an emitting surface may be 10 times that for cesium conduction. The measurements of cesium conduction heat transfer were always taken at a condition of no current flow in the test vehicle.

The procedure for taking the cesium conduction measurements is as follows:

1. The emitter temperature is set at 1735°C true; the collector root temperature is set at 465°C and an initial interelectrode spacing of some arbitrary value (e.g., 1 mil) is set.
2. The cesium reservoir temperature is set at some initial low value such as 300°C and the electron bombardment voltage-current is measured for the preset conditions of T_E = 1735°C (true), $T_{coll.\ root}$ = 465°C, and spacing of 1 mil.
3. Progressively increasing cesium reservoir temperatures are established and the increase in bombardment power to maintain the preset emitter temperature is recorded. The collector root temperature is fixed by a temperature controller which regulates the heater input power to the collector to account for the additional heat input via cesium conduction. Measurements were also taken by decreasing the cesium vapor pressure to reproduce the data.

The sources of possible error in these measurements are: reading accuracy of the meters which is about 0.5 percent, the spacing gages which are accurate to within ±0.0001 inch, and thermocouple readings of the reservoir which is a ±1 percent chromel-alumel thermocouple.

2.5.2 Measurement Results

Measurements were made according to the procedure outlined above for interelectrode spacings of 0.2, 0.5, 1, 2, and 3 mils, and cesium reservoir temperatures ranging from 573°K to 700°K. In all cases, the collector root temperature was preset and controlled at a constant 738°K while the emitter bombardment power was adjusted to maintain an emitter temperature of 2008°K.

The results of the measurements at the two closest spacings are shown in Table 2-IV. The cesium reservoir temperatures are shown in the first column and the corresponding cesium vapor pressures in the second column. The vapor pressures were calculated from the equation (Ref. 3):

$$\log P_{cs}\ (\text{torr}) = 6.91 - (3.80 \times 10^3)/T_{cs}$$

or

$$\log_{10} P_{mm} = 11.0531 - 1.35 \log_{10} T(^\circ K) - \frac{4041}{T(^\circ K)}$$

TABLE 2-IV

BOMBARDMENT POWER REQUIRED FOR T_e = 1735°C AS A FUNCTION OF T_{cs} FOR INTERELECTRODE SPACINGS OF 0.2 AND 0.5 MILS

		W = 0.2 mil		W = 0.5 mil	
T_{cs} (°K)	P_{cs} (torr)	H (W)	ΔH (W)	H (W)	ΔH (W)
573	1.9	261.9		257.4	
			15.5		17.5
603	4.1	271.6		271.9	
			10.9		10.0
617	5.5	277.4		274.9	
641	9.3	282.5		281.9	

The third and fifth columns show the total bombardment power delivered to the emitter to maintain the emitter at 1735°C at the indicated cesium reservoir temperatures for the spacings of 0.2 and 0.5 mils, respectively. Note that these values represent several power losses in addition to cesium vapor conduction losses and, therefore, their magnitudes are less important than their differences. The power differences between the first and third reservoir temperatures and the second and fourth reservoir temperatures are shown in the fourth and sixth columns. Since each power measurement is made by measuring bombardment current and bombardment voltage with a meter reading accuracy of 0.5 percent, the reading error is about 1 percent in the absolute magnitudes. This results in an error in the differences in power that can be as high as 2.5 watts.

The results of the measurements at the larger spacings are shown graphically in Fig. 2-21. The plotted points are power differences calculated from the measured power levels. Each curve is identified by the interelectrode spacing in mils. The errors in these data points are comparable to those of the close-spacing data of Table 2-IV, although the relative error is less. The solid lines are calculated from the semiempirical equation determined by Kitrilakis and Meeker (Ref. 4), with the constants shown in the figure.

2.5.3 Discussion of Results

Although all the cesium conduction measurements were made at relatively high cesium pressures from about 1 torr to 30 torr, there are two transport regimes represented by the data of Table 2-IV and Fig. 2-21. The data from the measurements at 0.2 and 0.5 mil spacings indicate a free-molecule transport while those made at the larger spacings indicate transport is occurring in the transition region between free-molecular and mass or viscous flow.

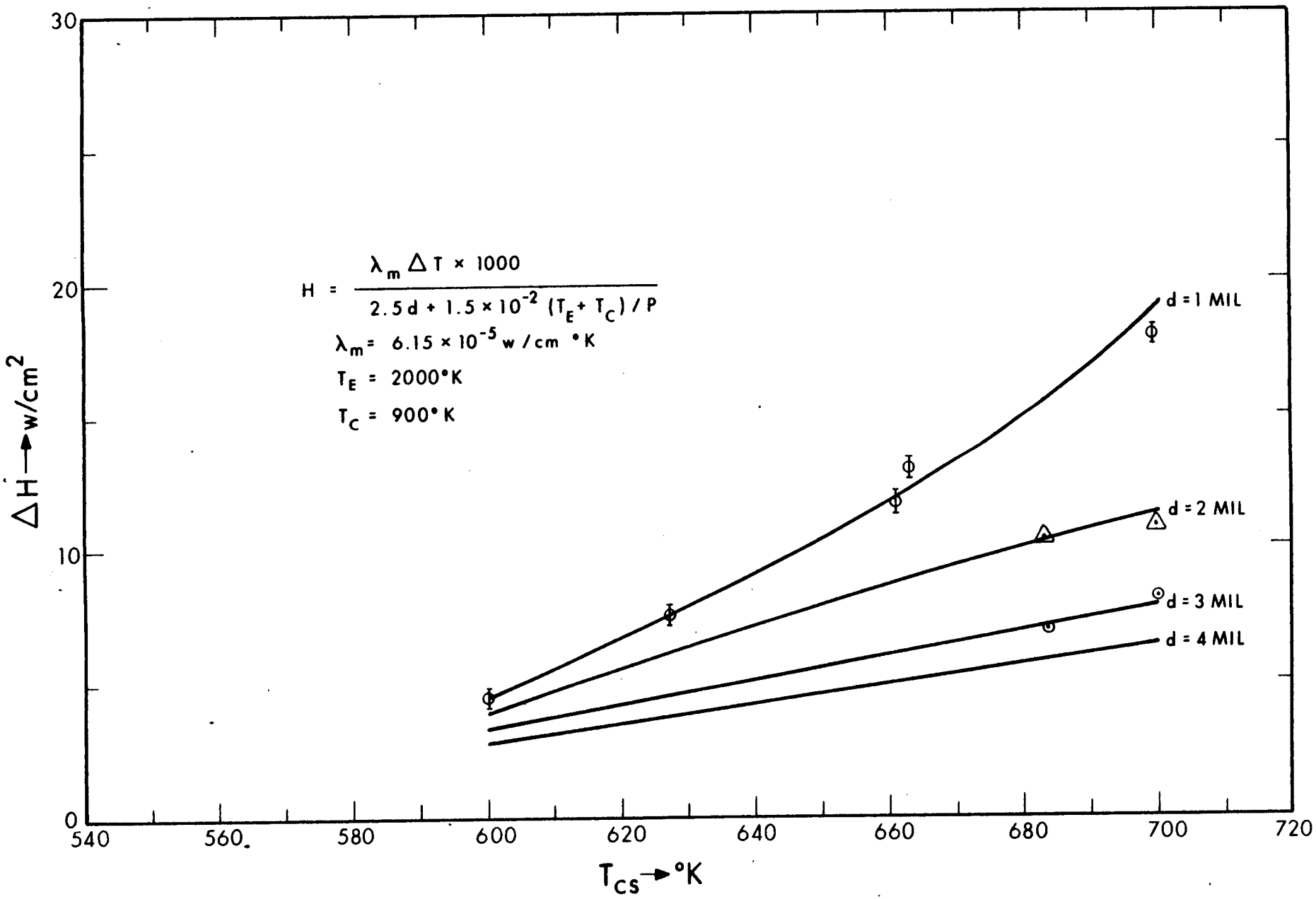

FIG. 2-21 CESIUM CONDUCTION MEASUREMENTS COMPARED WITH SEMI-EMPIRICAL THEORY

Free molecular heat transport will occur when the cesium mean free path is approximately equal to, or greater than, the interelectrode spacing and is characterized by its independence of spacing. This characteristic is shown by the power differences of Table 2-IV for the two close spacings. Within experimental error, these differences are identical although the spacings differ by a factor of 2.5. Estimates of the cesium mean free path based on hard-sphere interactions are consistent also with this interpretation. Assuming a cesium diameter of 4 to 7Å and cesium atom number densities ranging from $3.2 \cdot 10^{16}$ cm^{-3} at the lowest reservoir temperature to $1.4 \cdot 10^{17}$ cm^{-3} at the highest temperature, the mean free path ranges from a maximum of 1.7 mils for the low pressure and smaller diameter to 0.1 mil at the higher pressure and larger diameter. The equation used for these estimates is

$$L\ (cm) = (\sqrt{2}\ \pi\ \sigma^2\ n)^{-1}$$

where

σ = hard-sphere diameter

n = number density

For free-molecular transport, the heat flow between parallel plates for monatomic cesium is given by (Ref. 5):

$$H = 2\ \alpha_e\ \mu\ k\ S\ (T_e - T_c)$$

where

α_e = effective accommodation coefficient for heat transfer

μ = cesium arrival rate

k = Boltzmann's constant

S = area of the plates

T_e, T_c = emitter and collector temperatures

The arrival rate is calculated by

$$\mu = P_{cs}/(2\pi\, mkT)^{1/2}$$

where

m = mass of the cesium atom

P_{cs} = vapor pressure of cesium in the reservoir.

The appropriate temperature in this equation is the temperature at the point where the cesium enters the interelectrode region from the channel connecting this region and the reservoir. For the test vehicle, this temperature is the collector temperature. Using $T_e - T_c = 1.24 \cdot 10^3\ ^\circ K$ and $T_c = 760^\circ K$,

$$H\ (\text{watts}) = 3.8\, \alpha_e\, S\, P_{cs}$$

for P_{cs} in torr and S in cm^2. The difference, ΔH, between the heat conducted at two cesium pressures is

$$\Delta H = 3.8\, \alpha_e\, S\, \Delta\, P_{cs}$$

assuming constant α_e and S. Using the data of Table 2-IV for the four power differences shown, α_e S varies from 0.5 cm^2 to 1.3 cm^2 with an average of 0.9 cm^2. For an area of 2.4 cm^2, this indicates the effective accommodation coefficient is 0.4. This result, although based on data with considerable relative error, is consistent with the results of others (Ref. 6) for heat transport in the molecular flow regime. Since the accommodation coefficient at the low cesium coverages on the emitter at these temperatures and pressures is undoubtedly very close to unity, it is reasonable to conclude the value 0.4 is characteristic of the collector surface covered by at least one monolayer of cesium.

The data for spacings of 1 mil and larger has not been examined completely during this report period. However, within experimental error, it follows the predictions of the semiempirical equation of Kitrilakis and Meeker (Ref. 4). The results of these measurements will be investigated in detail in subsequent reports.

3. CONVERTER STUDY AND SECONDARY EXPERIMENTS

3.1 Interelectrode Spacing

A thermal mockup of a converter was fabricated with the same L/A ratio as the converter SN-101. The intention is to experimentally measure directly the at-temperature interelectrode spacing of the simulated converter.

This section will describe the interelectrode spacing vehicle, show theoretical calculations and show the experimental results. Spacing information from the test vehicle will be correlated to converter fabrication techniques.

3.1.1 Theoretical Calculations of the Converter Thermal Mockup

Figure 3-1 is a cross section of the interelectrode spacing vehicle thermal mockup. The emitter heat choke was machined to give a L/A ratio similar to that of a converter. It has a 0.003-inch-thick wall for a length of 0.200 inch.

$$L/A = \frac{0.200 \times 2.54}{3.14 \times 0.633 \times 3 \times 6.45 \times 10^{-3}}$$

$$L/A = \frac{5.08 \times 10^{-1}}{3.85 \times 10^{-2}}$$

$$L/A = 13.2 \text{ cm}^{-1}$$

To minimize the cost of the emitter heat choke it was made of tantalum rather than rhenium. The thermal expansion characteristics of tantalum are very similar to rhenium (Ref. Fig. 3-2).

In order to calculate the interelectrode spacing, a temperature distribution of the emitter heat choke was taken. Fig. 3-3 shows the temperature distribution of the envelope. The interelectrode

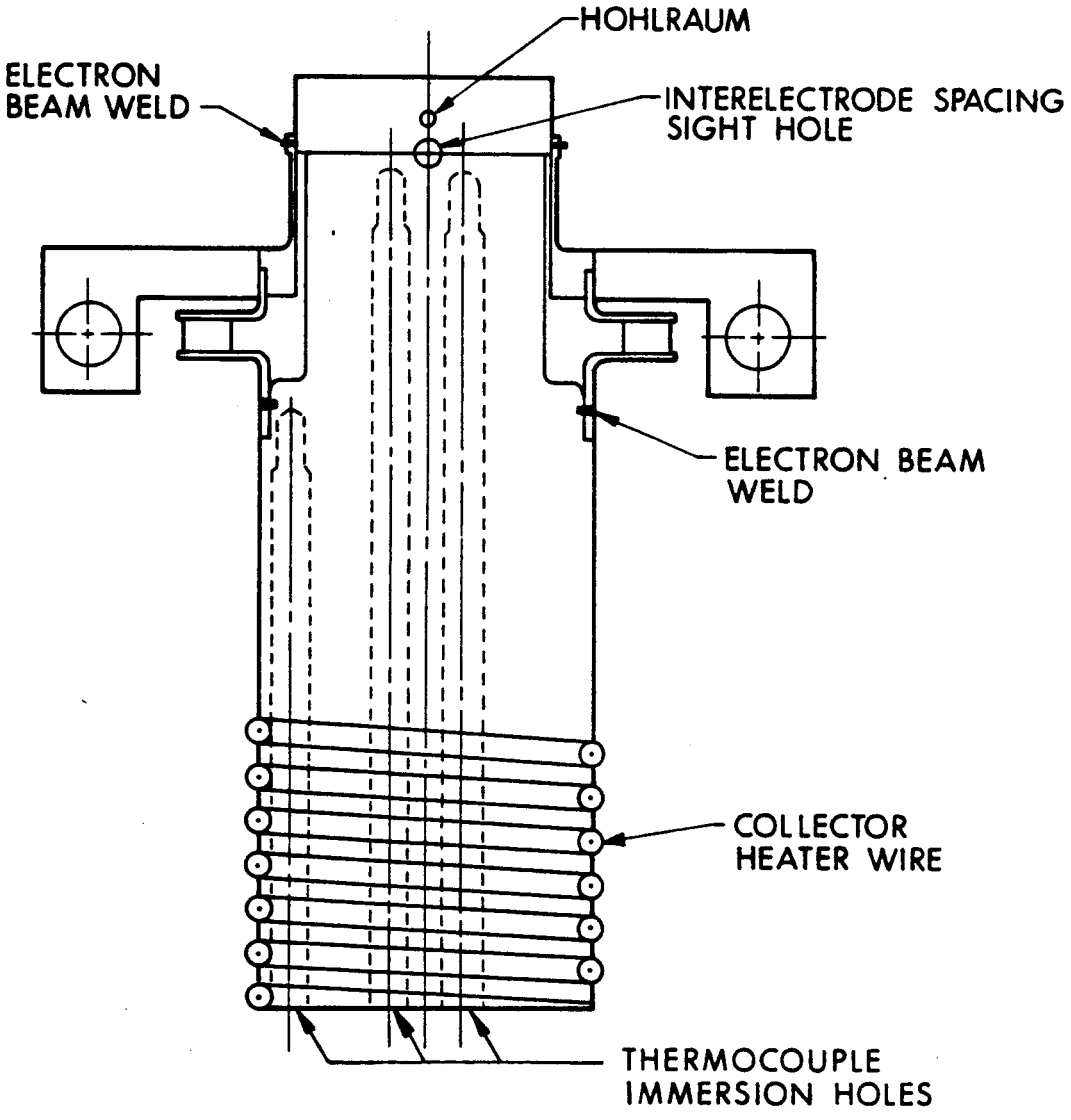

FIG. 3-1 THERMAL MOCK-UP FOR INTERELECTRODE SPACING MEASUREMENTS

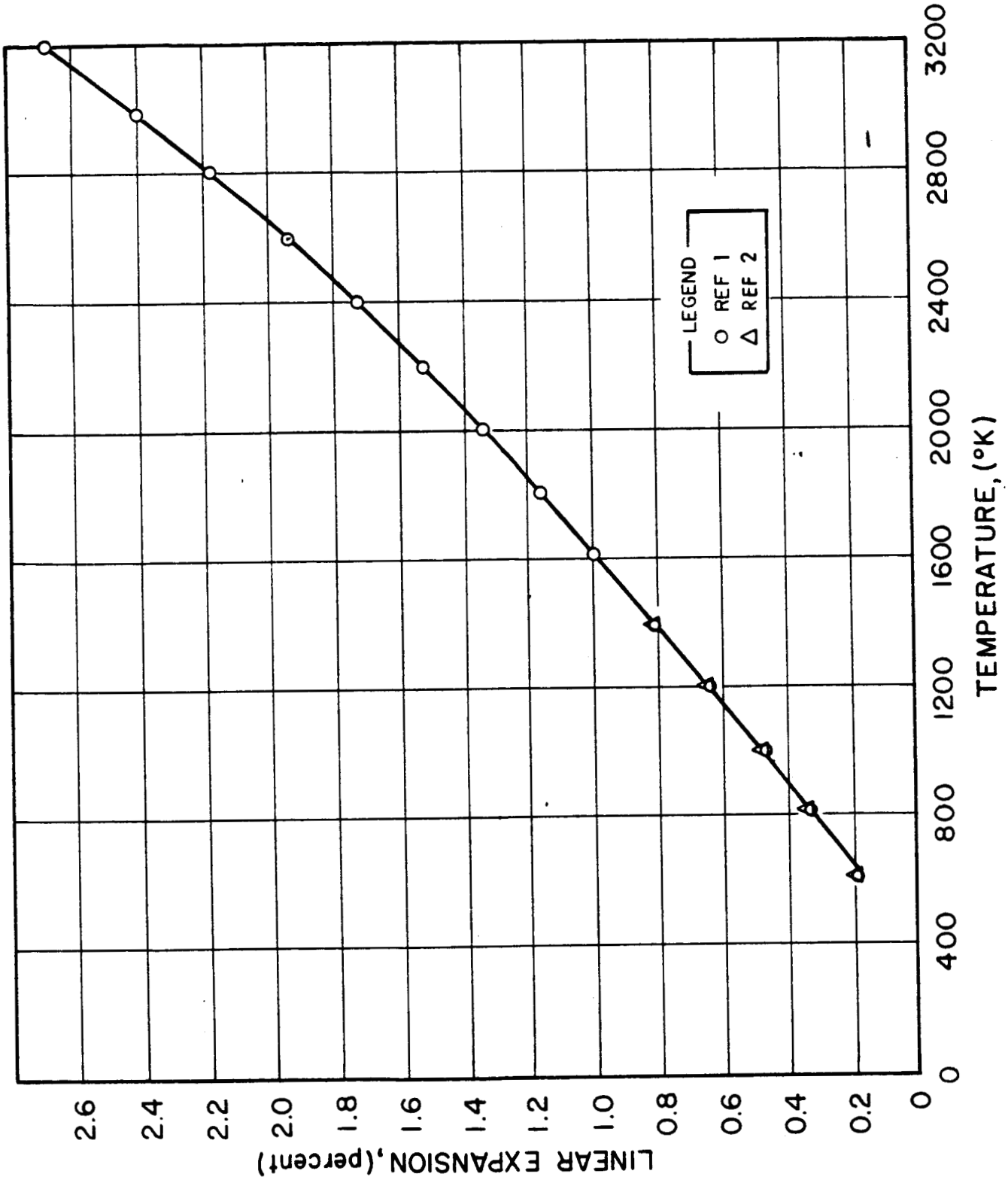

FIG. 3-2 COMPARISON OF TANTALUM AND RHENIUM THERMAL EXPANSION DATA

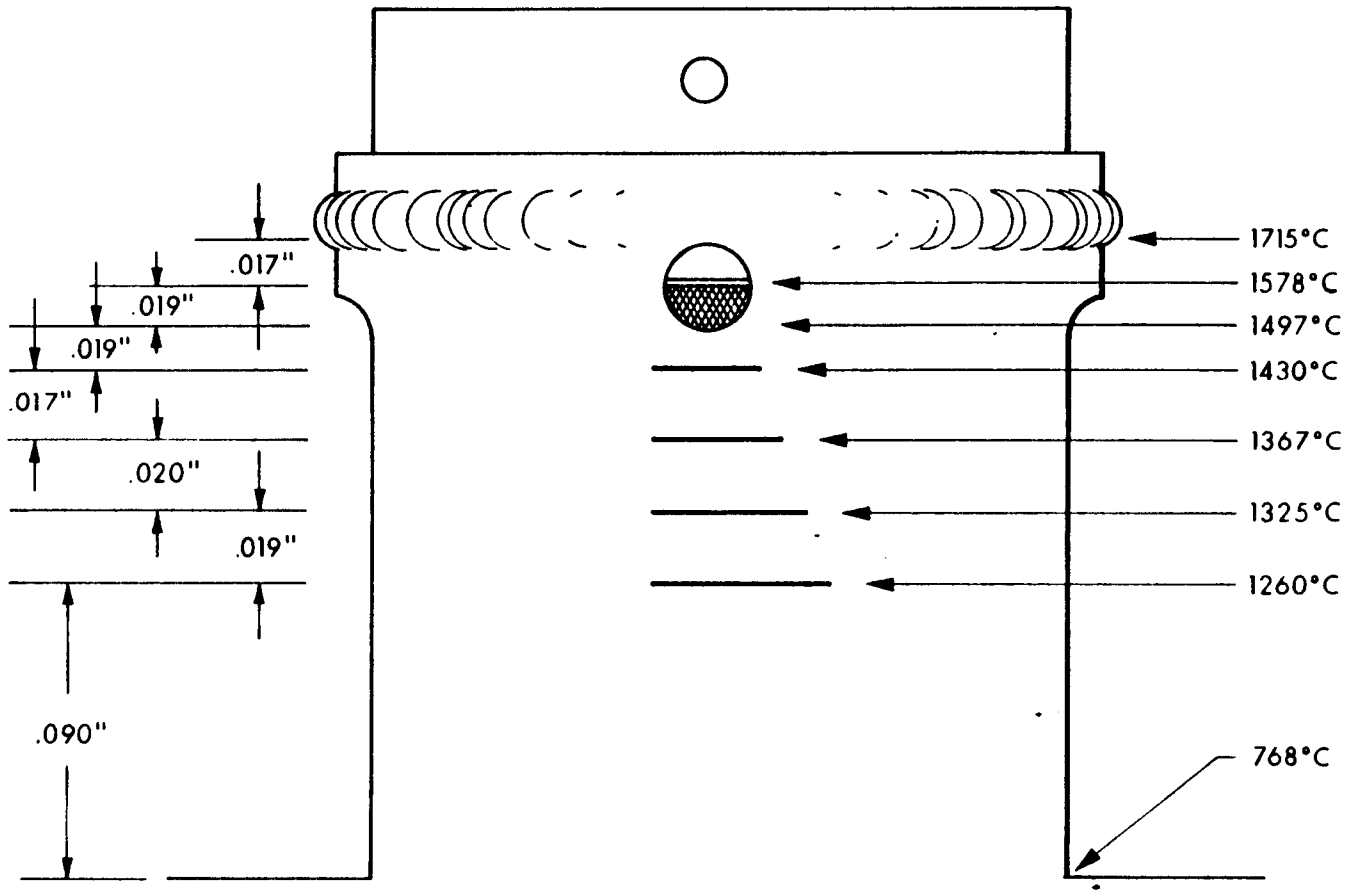

FIG. 3-3 EMITTER HEAT CHOKE TEMPERATURE (TRUE) DISTRIBUTION

spacing is the expansion of the emitter envelope plus the expansion of the seal minus the collector expansion. Assuming that the emitter at room temperature is stress-free, the thermal expansion of the emitter envelope can be calculated using a piece-wise solution. It is felt that a piece-wise solution is valid because sufficient number of pieces (seven) will be taken. The expansion is $\Delta l = lo\ \alpha\ \Delta T$, where Δl is the change in length, lo is the initial length at room temperature, α is the coefficient of thermal expansion of tantalum (Ref. 7) and ΔT is the change in temperature.

The total expansion of the envelope is a summation of the smaller members.

$$\Delta l = \Delta l_1 + \Delta l_2 + \Delta l_3 + \Delta l_4 + .-.-.- + \Delta l_7$$

$$\Delta l_1 = 01.7 \text{ inches} \times 1.27 \times 10^{-4} = 2.06 \times 10^{-4}$$

$$\Delta l_2 = 01.9 \text{ inches} \times 1.16 \times 10^{-4} = 2.20 \times 10^{-4}$$

$$\Delta l_3 = 01.9 \text{ inches} \times 1.10 \times 10^{-4} = 2.09 \times 10^{-4}$$

$$\Delta l_4 = 01.7 \text{ inches} \times 1.06 \times 10^{-4} = 1.80 \times 10^{-4}$$

$$\Delta l_5 = 02.0 \text{ inches} \times 1.01 \times 10^{-4} = 2.02 \times 10^{-4}$$

$$\Delta l_6 = 01.9 \text{ inches} \times 0.96 \times 10^{-4} = 1.82 \times 10^{-4}$$

$$\Delta l_7 = 09.0 \text{ inches} \times 0.7 \times 10^{-4} = \frac{6.30 \times 10^{-4}}{18.29 \times 10^{-4}}$$

Therefore, the calculated change in the emitter envelope is 0.00183 inch.

Likewise, the thermal expansion of the seal assembly can also be calculated. Assuming that the ceramic member has the same coefficient of thermal expansion as the niobium metal member, (Ref. 8) with an average seal temperature of 650°C, the α of niobium is 0.51×10^{-2}; for ≈ 0.50 inch we have

$$0.50 \text{ inch} \times 0.51 \times 10^{-2} = 0.0026 \text{ inch}$$

Therefore, the seal expansion is 0.0026 inch.

The molybdenum collector expansion for a collector measuring length (lo) of 0.650 inch, assuming an average collector temperature of 700°C, is $\alpha = 0.35 \times 10^{-2}$ (Ref. 9) and gives: $\Delta L_C = 0.650 \text{ inch} \times 0.35 \times 10^{-2} = 0.00228$ inch. Therefore, the calculated change in the interelectrode spacing is: $\Delta 5 = (0.00183 \text{ inch} + 0.0026 \text{ inch}) - 0.00228 \text{ inch} = 0.00215$ inch with an operating temperature of 1735°C on the emitter, an average collector temperature of 700°C, and a seal temperature of 650°C.

3.1.2 Direct Experimental Measurement of Interelectrode Spacing

Direct measurements of the interelectrode spacing were made by optically measuring the gap distance at temperature by sighting through a 0.038-inch-diameter hole which was drilled in the side of the emitter envelope assembly.

Figure 3-4 shows the testing setup. A self-contained 40-liter-per-second vacuum ion pump was used to minimize floor vibrations. Precision optical measurements are taken through an optically flat quartz window in a quartz bell jar. The spacing was directly measured by sighting through a Bausch and Lomb micrometer drum crosshair eyepiece mounted on a 75 power microscope. The micrometer drum was calibrated against a ruled micrometer stage (Bausch and Lomb 31-16-89). The established accuracy of this optical system is ± 0.0001 inch. The emitter temperature of the converter mockup was varied from 1250°C to 1800°C with an electron bombardment heater. The tantalum emitter has a 10:1 depth to diameter hohlraum for micro optical pyrometer temperature measurements.

The seal and envelope were fabricated as an assembly and electron-beam welded to the collector.

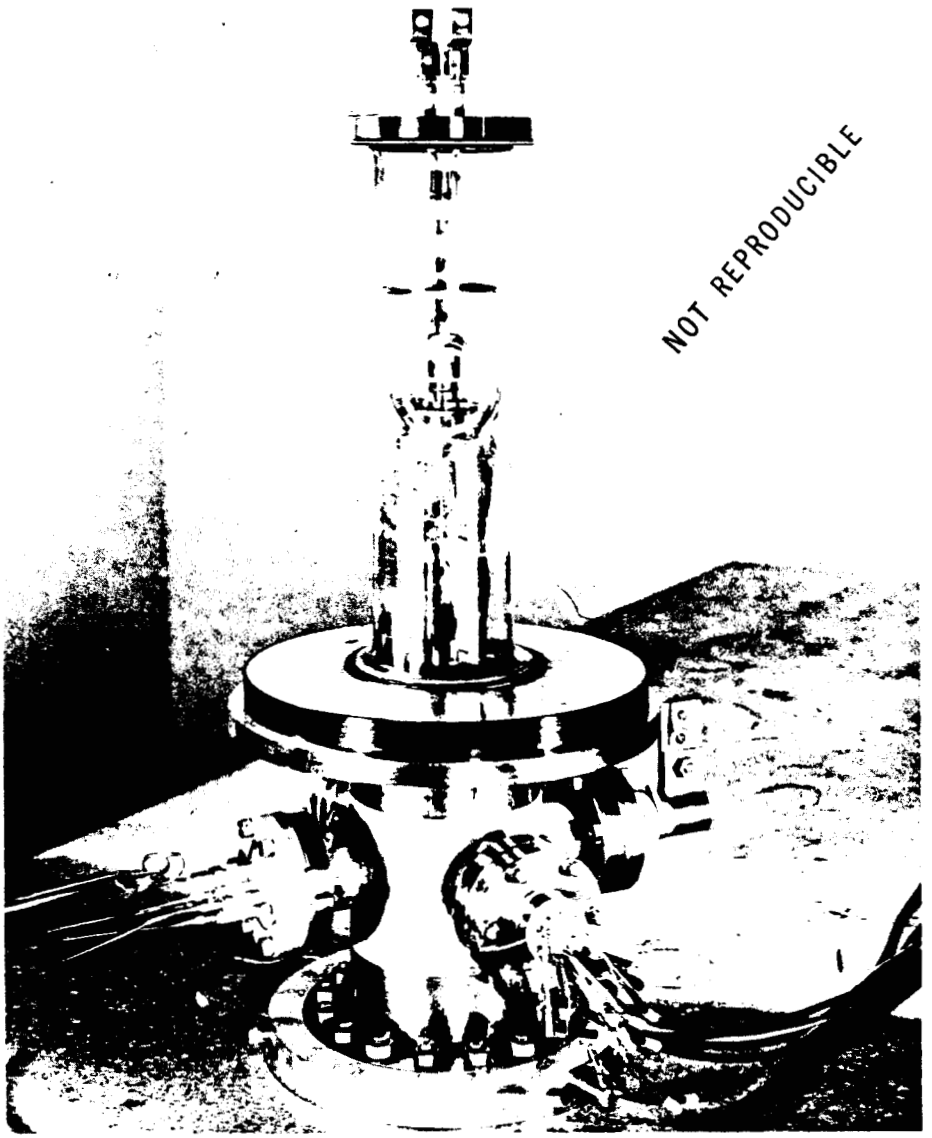

FIG. 3-4 SPACING EXPERIMENT SETUP. NOTE HIGH-QUALITY QUARTZ WINDOW FOR OPTICAL MEASUREMENTS

The molybdenum collector was bored to accommodate an immersion thermocouple. Tantalum sheathed heaters were brazed to the collector root. The heaters allow the average collector temperature to be varied in order to allow the determination of the effects of collector temperature on the interelectrode spacing.

The emitter collector spacing was set at 0.003 inch when fabricated. This spacing insures that the emitter envelope is in a stress free state at room temperature.

Distances between the emitter and collector were measured by focusing on the selected electrode and aligning the cross-hair of the micrometer drum at the surface of that electrode; the cross-hair was then moved, counting the number of drum revolutions, until it was aligned with the surface of the other electrode. This procedure was then reversed. At least six readings were taken at each set of parameters.

Direct optical determination of the spacing yielded variations up to 0.0002 inch from reading to reading. The variation in the readings is dependent upon the ability to precisely focus on the electrode faces when they are at temperature. A typical at-temperature picture of the gap region looking through the microscope is shown in Fig. 3-5. (The cross-hairs in the picture are out of focus to accommodate the camera.)

Figure 3-6 shows the change in interelectrode spacing for various emitter temperatures, and seal temperatures of 608 degrees and 650 degrees. The calculated change in interelectrode spacing of 0.0025 inch and the experimentally measured spacing changes of 0.0023 inch at $T_{emitter}$ = 1735, $T_{coll.}$ = 700°C, T_{seal} = 650°C show close agreement.

Calculated values for the spacing change cannot be more accurate than ± 5 percent, because the best published data available for the coefficient of thermal expansion (α) vary by this amount.

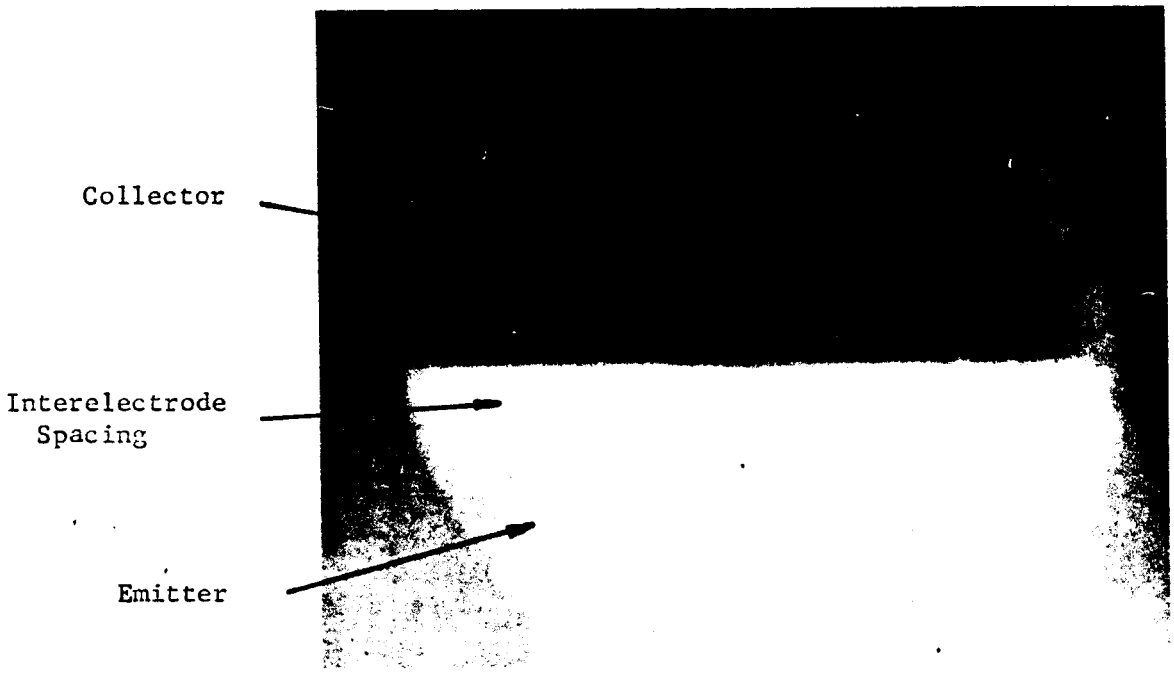

FIG. 3-5 PHOTOGRAPH OF INTERELECTRODE SPACING AT AN EMITTER TEMPERATURE OF 1735°C. $T_{COLLECTOR}$ = 700°C. INTERELECTRODE SPACING MEASURED TO BE 5.6 MILS

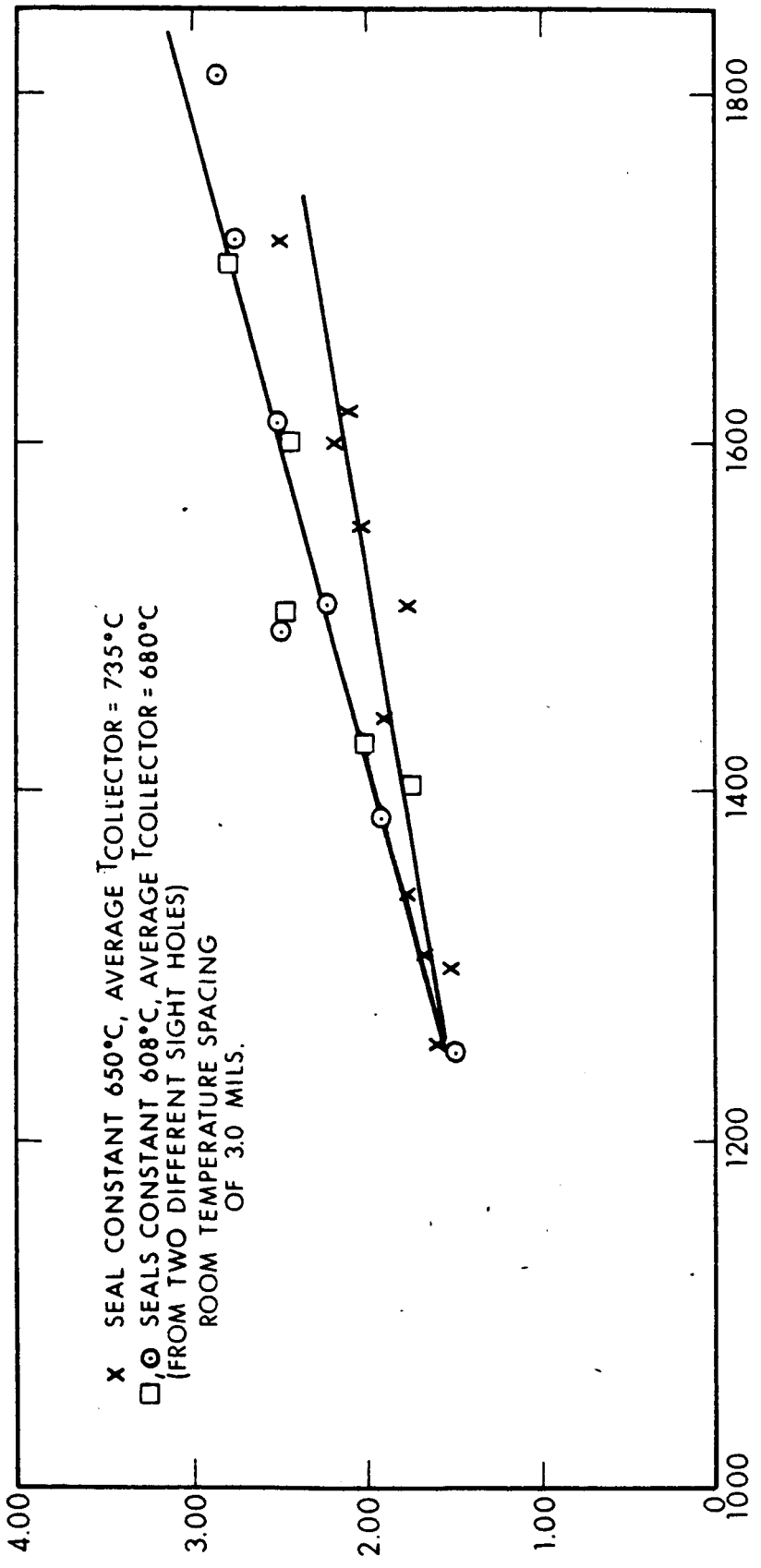

FIG. 3-6 CHANGE IN INTERELECTRODE SPACING AS A FUNCTION OF EMITTER TEMPERATURE

For example, 99.90 pure niobium has an α of 8.03 x $10^{-6}/^{o}C$, and 99.92 pure niobium has an α of 8.45 x $10^{-6}/^{o}C$. (Ref. 10). This variation in α is due to differences in the purity of the material involved. As a rule, the higher the purity of a particular material the larger its thermal expansion (α).

3.1.3 Problems in Achieving Precision Interelectrode Spacing in Thermionic Converter Hardware

In converter operation, a large ΔT is present in the collector due to the thermal load caused by the converter current. This ΔT must be considered when correlating the spacing data obtained from the interelectrode spacing device with an operating converter. At 50 ampere converter current with a 1.88 cm^2 collector cross section area, the ΔT in the molybdenum collector is 115°C. At 70 amperes converter current, the collector ΔT is 150°C.

When fabricating a converter, the ability to achieve an operating spacing that is accurate to ± 0.0001 inch is decidedly a function of the fabrication processes such as machine tolerances, annealing, electron-beam welding, and brazing.

One fabrication procedure entails electron-beam welding the emitter on the rest of the converter as the final subassembly step. This insures not only the desired spacing but also eliminates stress in the metal-to-ceramic seal. If the emitter-envelope subassembly is seal brazed to the collector subassembly as the final fabrication process, the spacing at operating temperature will be determined by variable brazing temperatures, variable braze run-out, and annealing state of flange materials. Also, if the emitter and collector surfaces are in contact the seal braze is made in compression, and variable stresses are induced in the seal and envelope.

A realistic tolerance for practical converter interelectrode spacings should be ± 0.0002 inch.

3.2 Electron-Beam Welding of Niobium to Niobium

An experimental investigation was conducted to examine the feasibility of electron-beam welding prefabricated ceramic-metal seals to the collector. Sample welds of niobium sheet were made to molybdenum plate to determine a schedule that resulted in good penetration into the molybdenum. A schedule of 150 kV x 4.2 mA at a part speed of 91 in./min yielded penetration through the 0.020 inch niobium sheet and approximately 0.025 inch into the molybdenum plate. A niobium flange was then welded to a molybdenum rod utilizing this schedule; however, the assembly leaked. A subsequent assembly also leaked. A niobium-niobium weld configuration was prepared by first brazing a niobium ring to a molybdenum bar and then electron-beam welding a 0.020 inch niobium flange to it. The resultant joint was leak tight and metallurgically examined for penetration. Figure 3-7 is a photograph of the weld indicating penetration through the flange and 0.020 inch into the backup ring.

There has been a notable lack of binary diagrams and information concerning the niobium-molybdenum system. Hansen (Ref. 11) devotes only a paragraph to niobium-molybdenum concluding that "Nb and Mo form an uninterrupted series of body centered cubic solid solutions." However, more recent work (Ref. 12) on the Nb-Mo system indicates:

1. Intermediate alloys of Nb-Mo contain large pores indicating that Nb-Mo and Mo-Nb diffusion rates in the melt are quite different.
2. An increase in hardness from 200 kg/mm for 100 percent molybdenum, to 420 kg/mm^2 for molybdenum with only 15 percent addition of niobium.

From this very preliminary survey it may be suspected that the electron-beam welding of Nb to Mo could be a marginal process since both materials are brought to their melting point in the weld zone with the attendant formation of a Nb-Mo alloy having properties substantially different than the two base materials.

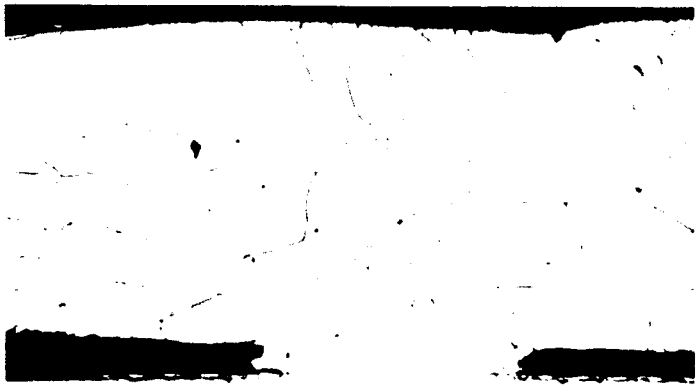

FIG. 3-7 ELECTRON-BEAM WELD OF 0.020-INCH THICK NIOBIUM RING TO 0.060-INCH THICK NIOBIUM RING. BEAM VOLTAGE OF 150 kV x CURRENT OF 2.8 mA. PART ROTATION SPEED OF 40 rpm (Mag 100X)

4. CONVERTER SN-101 (FABRICATION AND PROCESSING)

Converter SN-101 is being fabricated utilizing the data from the variable parameter test vehicle and information obtained from the secondary experiments. The electrodes are rhenium plate stock taken from the same mill run as those used in the test vehicle and processed in an identical manner. The interelectrode spacing of SN-101 is being set at 3.6 mils to obtain the optimum performance of 15.5 watts/cm^2 at 0.8 volt dc output for an emitter temperature of 1735°C (true). To obtain a spacing of 3.6 mils at temperature, the converter is being fabricated with a spacing of 0.0008 to 0.001 inch at room temperature. Since the rhenium emitter is the last part to be joined to the exhaust assembly, accurate height measurements of the emitter support structure and collector subassembly can be taken to grind a shoulder on the emitter circumference. This shoulder will form a butt joint with the envelope and allow the emitter to be self-fixtured during the E-B weld operation.

The electron beam welding operations for converter SN-101 are rhenium to rhenium and niobium to niobium. The rhenium weld is the attachment of the emitter to the emitter support structure. A weld schedule of 150 kV x 4.9 mA at a part speed of 80 in./min was found to produce good penetration welds and remain leak tight through repeated thermal cycle. The niobium weld allows the ceramic-metal seals to be prefabricated, leak checked and then joined to the envelope/collector subassemblies. In this manner the converter fabrication reliability is increased and the interelectrode spacing can be accurately preset.

The ceramic-metal seals are being prefabricated by joining niobium flanges to high purity alumina with Ni-Zr braze material. A flange thickness of 0.020 inch was chosen to improve the mechanical stability of the seal structure and consequently, the vibration

resistance. Sample seals have been thermal-cycled at a rate of 100°C/min for 250 cycles and remained leak tight when tested with a helium mass spectrometer of 5×10^{-10} cc-atom/sec sensitivity. These same seals have been operated at 700°C for 500 hours, determined to be leak tight and returned to test for an additional 1000 hours.

Converter SN-101 is presently being assembled by joining the prefabricated seal structure to the collector and emitter envelope subassemblies as shown in Fig. 4-1. The copper radiator fin structure is joined, in compression, to the molybdenum collector with a nickel-gold alloy which was extensively tested for thermal integrity and determined to be satisfactory. It has been calculated that 200 thermal watts can be dissipated by this system corresponding to a steady state 70 ampere operation. For lower current levels, separate heater units are mechanically attached to the fins to allow for parametric optimization.

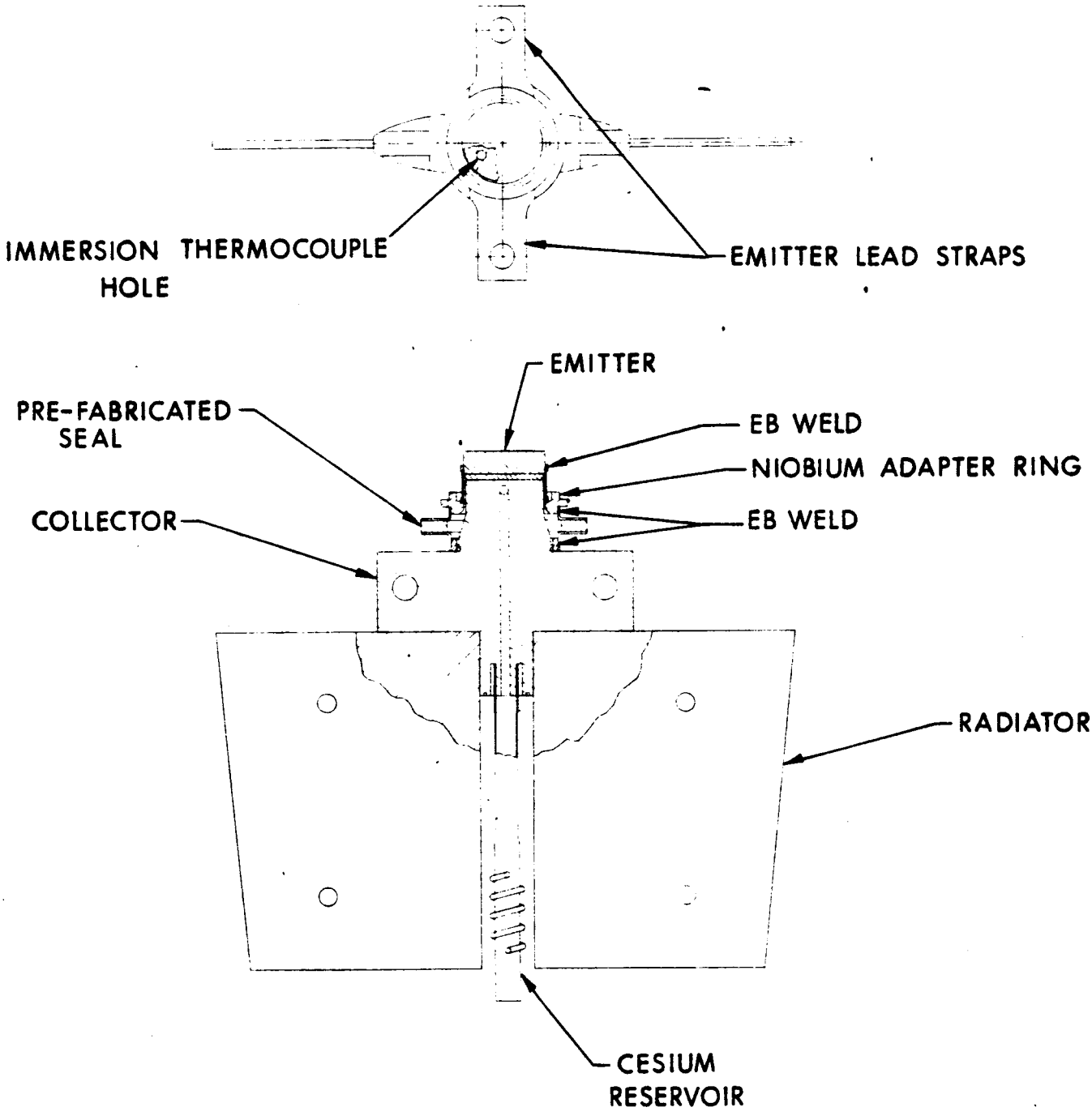

FIG. 4-1 CONVERTER SN-101 ASSEMBLY

5. PROGRAM FOR NEXT QUARTER

5.1 Variable Parameter Test Vehicle

Evaluation of the rhenium-rhenium electrode system will be concluded by acquiring the rest of the 0.7V and 0.6V dc converter optimization data. In addition, more pd curves will be obtained and analyzed. After the rhenium-rhenium system is completed, a rhenium-molybdenum system will be evaluated in the same depth.

5.2 Secondary Experiments

The operation of a niobium-zirconium brazed, ceramic-metal seal will be terminated after 2000 hours at 700°C. After leak check, the seal assembly will be metallurgically examined.

5.3 Converter Design, Fabrication and Test

The converter design and fabrication will proceed with data from the variable parameter vehicle and converter secondary experiments. Converter SN - 101 will have a rhenium-rhenium electrode system spaced at 3.6 mils for maximum power output at 0.8V dc.

REFERENCES

1. D. H. Pollock, IEEE Thermionic Conversion Specialist Conference, San Diego 1965
2. A. O. Jensen, A. E. Campbell, and W. Dong, IEEE Thermionic Conversion Specialist Conference, Gatlinburg, 1963
3. Saul Dushman, Scientific Foundations of Vacuum Technique, John Wiley and Sons, Inc., New York, second edition, p. 700 1962
4. S. Kitrilakis, and M. Meeker, "Experimental Determination of the Heat Conduction of Cesium Gas," Advanced Energy Conversion 3, 59-68 1963
5. Earle H. Kennard, Kinetic Theory of Gases, McGraw-Hill Book Company, Inc., New York, p 315ff 1938
6. W. R. Martini, "Theoretical Calculation of the Thermal Conductivity of Cesium Vapor at Thermionic Temperatures," Advanced Energy Conversion 3, 49-58 1963
7. Edwards, Speiser, Johnston, J. Appl. Phys., 22, April 1951
8. J. Tottle, Inst. Metals, 85, April 1957
9. "The Reactor Handbook," Vol 3, Sec 1, March 1955
10. G. L. Miller, "Metallurgy of the Rarer Metals," p. 350
11. M. Hansen, "Constitution of Binary Alloys," McGraw-Hill Book Company, Inc., 1958
12. V. N. Eremenko, Ukrain. Khim. Zhur, 20, 227-231, 1954